Serviceability Limits of Reinforced Concrete Hinges

Thomas Schlappal[a], Johannes Kalliauer[a], Markus Vill[b], Susanne Gmainer[c,d], Herbert Mang[a,e], Josef Eberhardsteiner[a], Bernhard Pichler[a,*]

[a] *TU Wien – Vienna University of Technology, Institute for Mechanics of Materials and Structures, Karlsplatz 13/202, AT-1040 Vienna, Austria*
[b] *Vill Ziviltechniker GmbH, Hermanngasse 18, AT-1070 Vienna, Austria*
[c] *Smart Minerals GmbH, Franz-Grill-Straße 9, AT-1030 Vienna, Austria*
[d] *Camillo Sitte Lehranstalt, Leberstraße 4c, AT-1030 Vienna, Austria*
[e] *Tongji University, College of Civil Engineering, Siping Road 1239, CN-200092 Shanghai, China*

This document is the accepted version of a work that was published in Engineering Structures. To access the final edited and published work see, `http://doi.org/dhz7`.

Abstract

Concrete hinges are monolithic necks in reinforced concrete structures. The serviceability limit states addressed herein refer to the open question how to limit tolerable relative rotations as a function of the compressive normal force transmitted across the neck. Analytical formulae are derived in the framework of the Bernoulli-Euler hypothesis and of Hooke's law. The usefulness of corresponding dimensionless design diagrams is assessed based on experimental data taken from the literature and on new results from structural testing of reinforced concrete hinges. This way, it is shown that the proposed mechanical model is suitable for describing serviceability limit states. Corresponding design recommendations are elaborated and exemplarily applied to verification of serviceability limit states of the reinforced concrete hinges of a recently built integral bridge. Because the reinforcement is explicitly accounted for, the tolerable relative rotations are larger than those according to the guidelines of Leonhardt and Reimann. Bending-induced tensile macrocracking beyond one half of the smallest cross-section of the neck is acceptable, because the tensile forces carried by the reinforcement ensure the required position stability of the hinges.

Keywords: serviceability limit states (SLS), integral bridges, design recommendations

1. Introduction

Concrete hinges were invented by Freyssinet [1, 2]. They are unreinforced or marginally reinforced necks in reinforced concrete structures. Practical applications include supports in integral bridge construction, see Fig. 1, and interfaces of segmental tunnel rings, see Fig. 2.

The present paper is devoted to reinforced concrete hinges, characterized by a few pairs of crossing steel rebars running across the neck, with cross-over points at the *centerline* of the neck (y, $x = z = 0$). The open question [3] regarding tolerable relative rotations $\Delta\varphi$ as a function of the normal force N trans-

*Corresponding author
Email address: `bernhard.pichler@tuwien.ac.at` (Bernhard Pichler)

mitted across the neck is tackled in the context of serviceability limit states.

As for testing of concrete hinges, with the aim to measure the relative rotation resulting from the bending moment and the compressive normal force transmitted across the neck, the following test protocol is typically used. Concrete hinges are subjected to a specific normal force, which is kept constant, and to a monotonously increased bending moment. As regards unreinforced concrete hinges, such test were carried out by Dix [5], Leonhardt and Reimann [6], as well as Franz and Fein [7]. Reinforced concrete hinges were tested by Tourasse [8], Base [9], Fessler [10], and Hordijk and Gijsbers [11]. These tests demonstrated that the relationship between bending moment and relative rotation is nonlinear, particularly because of progressive bending-induced tensile cracking in the neck region. An alternative testing protocol was used by Schlappal et al. [12], who carried out eccentric compression tests. These tests demonstrated that concrete hinges are highly creep-active structural elements and that creep and cracking of reinforced concrete hinges are coupled phenomena. In the present paper, new experimental data are presented. They refer to *reinforced* concrete hinges subjected to either eccentric compression or cycling bending at a constant normal force.

Available models for prediction of the relative rotation as a function of the bending moment and the normal force transmitted across the neck, can be categorized according to (i) their application either to bridge construction or to mechanized tunneling and (ii) the treatment of the reinforcement, which is either disregarded or explicitly considered. As for applications to bridge construction, Leonhardt and Reimann [6] set the tensile strength of concrete equal to zero. They accepted tensile macrocracking as long as it is limited to one half of the smallest cross-section. Along the remaining ligament, a *linear* distribution of compressive normal stresses was assumed. The compressive strength of concrete was increased relative to the uniaxial compressive strength, in order to account for the triaxial compressive stress states developing in the neck region. Kaufmann et al. [3], in turn, assumed a *nonlinear* distribution of the compressive stresses in the neck region and estimated these stresses, based on an approximate solution for a spread foundation resting on an elastic half space. In both approaches the steel rebars, if existing, are not accounted for. As for applications to mechanized tunneling, the available models for *un*reinforced concrete hinges mainly differ in the constitutive law used for concrete subjected to compression. Janßen [13] applied the approach of Leonhardt and Reimann [6]. This underlined that tubbing-to-tubbing interfaces of segmental tunnel linings show a similar structural performance as concrete hinges used in integral bridge construction. Another elasto-brittle model was developed by Gladwell [14]. It is based on the elastic contact problem of a flat punch, pressed unsymmetrically into a half space. A purely plastic approach, based on spatially uniform compressive normal stresses, was proposed by Caratelli et al. [15]. Linear-elastic *and* ideally-plastic behavior of concrete was accounted for by Blom [16]. The parabolic-rectangular stress-strain relationship, provided by the Eurocode 2 [17], was used by Tvede-Jensen et al. [18]. *Reinforced* concrete hinges in mechanized tunneling are interfaces, across which the neighboring segments are connected by steel bolts. Only few models account explicitly for these bolts. They mainly differ in the constitutive law used for concrete subjected to compression. A linear-elastic, ideally-plastic constitutive law was used by Zhang et al. [4] and a parabolic stress-strain relation by Liu et al. [19]. The parabolic-rectangular stress-strain relationship from the Eurocode 2 [17] was used by Li et al. [20, 21]. These models underline that computational expenses are increasing significantly with increasing level of advancement of the constitutive law used for modeling of concrete. The mentioned models for bolted interfaces were treated *numerically*, because closed-form analytical solutions were out of reach. The present paper is devoted to the extension of the approach of Leonhardt and Reimann [6] towards explicit consideration of centrically crossed steel rebars, with the aim to derive closed-form *analytical* formulae for serviceability limits of reinforced concrete hinges.

As for the design of concrete hinges in the framework of the deterministic design concept of the 1960s, pioneering guidelines for integral bridges were devel-

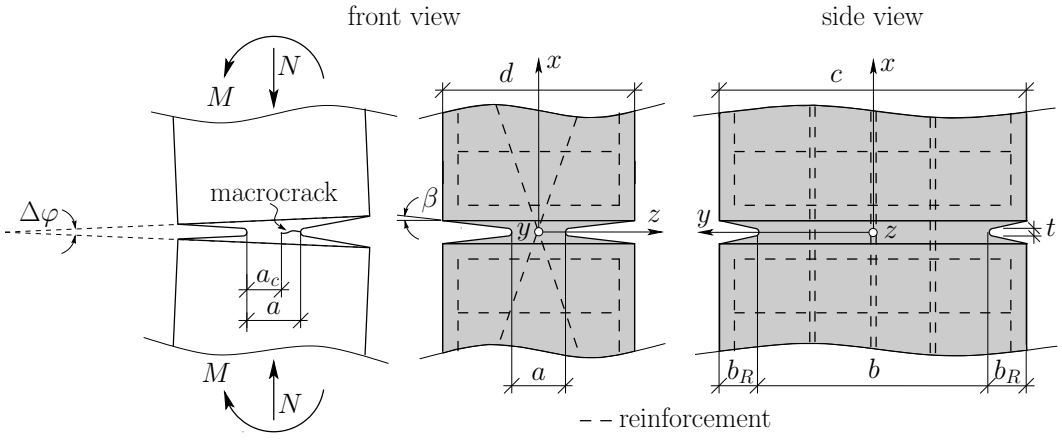

Figure 1: Geometric dimensioning of a concrete hinge with reinforcement crossing at the centerline of the neck; a_c denotes the width of the compressed ligament

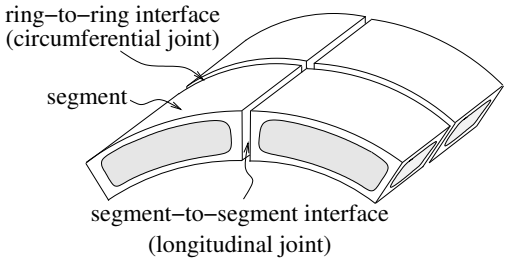

Figure 2: Segment-to-segment interfaces (also referred to as "longitudinal joints") and ring-to-ring interfaces (also referred to as "circumferential joints") [4]

oped by Leonhardt and Reimann [6], see also [22]. There, the maximum tolerable relative rotation $\Delta\varphi_\ell$ is bounded by the condition that tensile macrocracking is limited to one half of the width of the neck, estimated by means of the Bernoulli-Euler hypothesis and Hooke's law. This condition became part of obligatory design standards in the United Kingdom, see [23]. In the context of *ultimate* limit states, Marx and Schacht [24, 25] translated the guidelines of Leonhardt and Reimann [6] into the nomenclature of the semi-probabilistic safety concept of current European design standards. As for the design of interfaces of segmental tunnel rings, Janßen [13] applied the guidelines of Leonhardt and Reimann [6] in the context of *ultimate* limit states. These recommendations are popular up to date [26, 27]. Tvede-Jensen et al. [18] took the parabolic-rectangular stress-strain relationship from the Eurocode 2 [17] in order to derive a nonlinear relation between the bending moment and the relative rotation as the basis for determination of both serviceability and ultimate limit states of unreinforced concrete hinges. Still, the tolerable relative rotation has remained an unsolved issue [3], particularly when it comes to the treatment of serviceability limit states. Empirical solutions, based on experimental data from *short-term* structural testing, see the French code [28], appear to be incomplete when it comes to the assessment of the *long-term* behavior of concrete hinges. In addition, there is a need for design recommendations that account explicitly for the reinforcement. This is setting the scene for the present paper.

The objectives of this paper are (i) to address the open question how to limit tolerable relative rotations as a function of the compressive normal force transmitted across the neck of reinforced concrete hinges and (ii) to resolve the lack of analytical models for concrete hinges, which explicitly account for the load-carrying behavior of the reinforcement, provided that bending-induced tensile cracking extends across more than one half of the width of the neck. To this end, two types of serviceabil-

ity limits are investigated: either the steel rebars start to yield in tension or the maximum compressive normal stress of concrete reaches the triaxial compressive strength, or both occur simultaneously. The triaxial compressive strength of concrete is estimated, by analogy to [18, 24, 25, 29], based on regulations regarding partially loaded areas taken from the Eurocode 2 [17]. The proposed mechanical model employs the Bernoulli-Euler hypothesis and Hooke's law, whereby the tensile strength of concrete is set equal to zero. These idealizations are consistent with the approach of Leonhardt and Reimann [6]. Different operating conditions of reinforced concrete hinges are investigated. This includes " compression-dominated operation ", "tensile macrocracking up to one half of the width of the neck", "tensile macrocracking beyond one half of the width of the neck, resulting in tensile loading of the reinforcement", and "tension-dominated operation". The two latter scenarios exceed the limit of applicability of the design guidelines of Leonhardt and Reimann [6]. The described mechanical model is used to derive analytical formulae as the basis for dimensionless diagrams which illustrate the limits of the tolerable relative rotation as a function of the transmitted normal force. The formulae and, hence, the dimensionless diagrams can be specified for specific geometric and material properties of reinforced concrete hinges. Because the approach is based on several simplifying assumptions and idealizations, see above, the usefulness of the described approach is assessed with the help of experimental data taken from the open literature *and* of new results from structural testing of reinforced concrete hinges subjected to either eccentric compression or cyclic bending at a constant normal force. Subsequently, recommendations for verification of serviceability limit states of reinforced concrete hinges are elaborated. They are applied to *a posteriori* verification of serviceability limit states of a recently built integral bridge in Austria [30]. Ultimate limit states, in turn, are the focus of the companion paper [31].

The present paper is structured as follows. Section 2 contains the theoretical description of serviceability limits of reinforced concrete hinges. Section 3 is devoted to the assessment of the derived formulae by means of experimental data taken from the open literature *and* of new results from structural testing. Section 4 is devoted to recommendations for verification of serviceability limit states of reinforced concrete hinges and of their application to the aforementioned bridge. The paper ends with a discussion (Section 5), followed by conclusions (Section 6).

2. Theoretical investigation of serviceability limits of concrete hinges

The present study deals with double-symmetric reinforced concrete hinges, geometrically described by means of Cartesian coordinates x, y, z, see Fig. 1. In this illustration, a denotes the width and b the depth of the neck, b_R stands for the depth of the front-side notches, c for the depth of the adjacent reinforced concrete parts, and d for their width, t denotes the height of the throat of the neck, and β stands for the opening angle of the throat of the neck.

The rotational capacity of reinforced concrete hinges is governed by the normal force N, transmitted across the neck. This is the motivation to derive analytical formulae, expressing N as a function of both the change of length in the x-direction, $\Delta\ell$, and the relative rotation $\Delta\varphi$. Thereby, $\Delta\ell > 0$ indicates an elongation of the neck region, whereby $\Delta\ell < 0$ signals a shortening, see Fig. 3. In the context of a displacement-controlled analysis, both $\Delta\ell$ and $\Delta\varphi$ are imposed onto the neck of a reinforced concrete hinge, see Fig. 3. To this end, the neck region is idealized as a cuboid with geometric dimensions a, b, and a in the x, y, and z-direction, respectively, see Fig. 3.

2.1. Derivation of an expression for N as a function of $\Delta\ell$ and $\Delta\varphi$

The Bernoulli-Euler hypothesis is used to express the axial displacement field u and the axial normal strain ε, respectively, as a function of $\Delta\ell$ and $\Delta\varphi \ll 1$. This is similar to the approach of Leonhardt and Reimann [6] who employed this hypothesis implicitly in the context of unreinforced concrete hinges. Thus, u is obtained as

$$u = \Delta\ell \, \frac{x}{a} + \Delta\varphi \, \frac{x}{a} \, z \,, \tag{1}$$

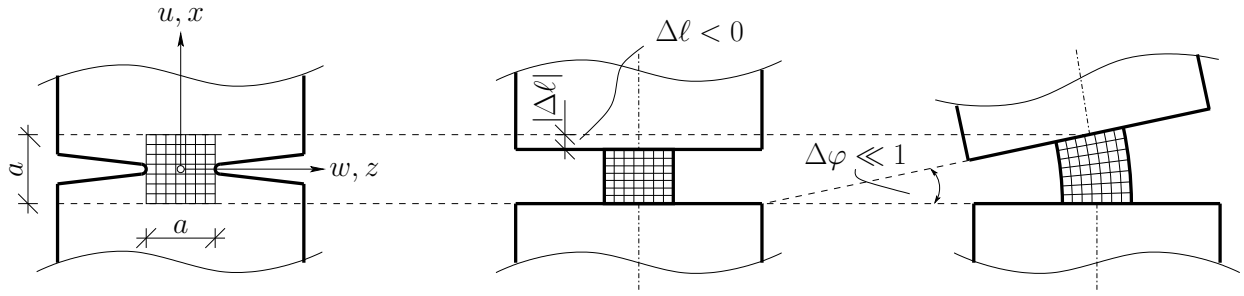

Figure 3: Idealized concrete hinge subjected to axial shortening $\Delta\ell < 0$ and to a relative rotation $\Delta\varphi$; the out-of-plane dimension b of the neck is not shown

see Fig. 3. Inserting Eq. (1) into the expression for the axial normal strain,

$$\varepsilon = \frac{\partial u}{\partial x}\,, \tag{2}$$

delivers the following expression for ε as a function of $\Delta\ell$ and $\Delta\varphi$:

$$\varepsilon = \frac{\Delta\ell}{a} + \frac{\Delta\varphi}{a}\,z\,. \tag{3}$$

Eq. (3) underlines that the slope of ε along the z-axis is proportional to $\Delta\varphi$:

$$\frac{\partial\varepsilon}{\partial z} = \frac{\Delta\varphi}{a}\,. \tag{4}$$

In order to calculate the axial normal stresses in the neck region, the material behavior of concrete and steel is idealized as follows. For the sake of simplicity, it is assumed that concrete is unable to carry tension:

$$\sigma_c = 0 \quad \ldots \quad \varepsilon_c \geq 0\,. \tag{5}$$

Linear elasticity up to the elastic limit stress[1] $|Ff_c|$ is assumed for concrete subjected to compression:

$$\sigma_c = E_c\,\varepsilon \quad \ldots \quad 0 \geq \varepsilon_c \geq -\frac{|Ff_c|}{E_c}\,, \tag{6}$$

where E_c is Young's modulus of concrete, see Fig 4 (a). As for the steel, the reinforcement is assumed to have a significant influence on the structural behavior only if subjected to tension. In case of tension, steel is assumed to behave in a linear-elastic fashion up to the yield stress f_y,

$$\sigma_s = E_s\,\varepsilon_s \quad \ldots \quad 0 \leq \varepsilon_s \leq \frac{f_y}{E_s}\,, \tag{7}$$

while compressive stresses of steel are disregarded:

$$\sigma_s = 0 \quad \ldots \quad \varepsilon_s \leq 0\,, \tag{8}$$

where E_s is Young's modulus of steel, see Fig 4 (b). Since the steel rebars run across the *centerline* of the neck (y, $x = z = 0$), their axial normal strain follows

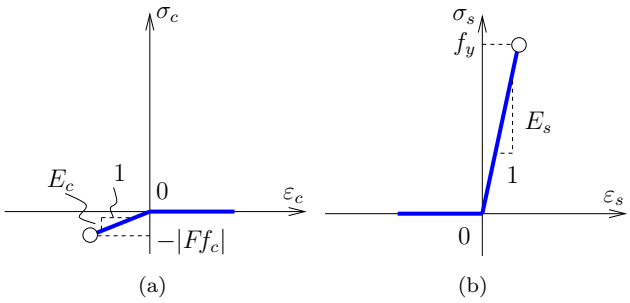

Figure 4: Linear-elastic material behavior of (a) concrete and (b) steel; σ_c, ε, E_c, and $|Ff_c|$, denote the normal stress, the normal strain, Young's modulus, and the compressive strength, respectively, of concrete; σ_s, ε_s, E_s, and f_y stand for the normal stress, the normal strain, Young's modulus, and the yield stress, respectively, of steel

[1] The elastic limit stress $|Ff_c|$ is discussed at the end of this Subsection.

from inserting $z = 0$ into Eq. (3) as

$$\varepsilon_s = \frac{\Delta\ell}{a}\,. \tag{9}$$

The normal force N, which is transmitted across the neck, is equal to the integral of the axial normal stresses over the cross-sectional area A of the neck:

$$N = \int_A \sigma \; \mathrm{d}A\,. \tag{10}$$

$\mathrm{d}A$ in Eq. (10) is equal to $b\,\mathrm{d}z$, where b denotes the constant out-of-plane dimension of the neck, see Fig. 1. The width of the compressed ligament of concrete is denoted as a_c, see Fig. 1. Thus, the integration along the z-direction is carried out from $-a/2$ to $-a/2 + a_c$:

$$N = \int_{-a/2}^{-a/2+a_c} \sigma_c\, b \; \mathrm{d}z + \sigma_s \, A_s \, \chi\,. \tag{11}$$

The second term on the right-hand-side of Eq. (11) refers to the reinforcement, with A_s denoting the cross-sectional area of the rebars running across the neck. The factor χ is equal to 1 in case of tensile loading, and equal to 0 otherwise, i.e.

$$\chi = \begin{cases} 1 & \ldots \quad \Delta\ell > 0\,, \\ 0 & \ldots \quad \Delta\ell \leq 0\,. \end{cases} \tag{12}$$

Inserting Eqs. (5)-(8) into Eq. (11), and specializing the resulting expressions for Eqs. (3) and (9) yields the sought expression for N as a function of $\Delta\ell$ and $\Delta\varphi$ as

$$\begin{aligned} N \;\; = \;\; & \frac{E_c\, b\, a_c}{a} \left[\Delta\ell + \frac{\Delta\varphi}{2}(a_c - a) \right] \\ & + E_s \, \frac{\Delta\ell}{a} \, \rho \, a b \, \chi\,, \end{aligned} \tag{13}$$

where ρ denotes the reinforcement ratio:

$$\rho = \frac{A_s}{ab}\,. \tag{14}$$

In Eq. (14), ab denotes the cross-sectional area of the neck, see Fig. 1.

The degree of utilization, ν, is introduced in order to transform N into a dimensionless quantity. To this end, N is divided by the maximum bearable compressive normal force:

$$\nu = \frac{N}{-|F f_c|\, ab} \leq 1\,. \tag{15}$$

The denominator in Eq. (15) follows from Eq. (13), specialized for pure compression of the neck ($\Delta\varphi = 0$, $a_c = a$, and $\chi = 0$), whereby the axial shortening $\Delta\ell$ is set equal to $-a\,|F f_c|/E_c$, such that $\varepsilon = -|F f_c|/E_c$ and $\sigma_c = -|F f_c|$, see Eqs. (3) and (6), respectively.

Finally, the elastic limit stress of concrete, $|F f_c|$, is discussed. In compression, concrete is idealized as linear-elastic up to a stress that is by a multiplicative factor F *larger* than the uniaxial compressive strength f_c. This is motivated by recently performed Finite Element simulations [29]. They have shown that the stress state in the neck is characterized by compressive normal stresses in the y-direction and z-direction in addition to the ones in the x-direction. The corresponding confinement pressure results in a significant strengthening of the concrete. Thus, F can be interpreted as the ratio of triaxial-to-uniaxial compressive strength. In the present context, this ratio is estimated, based on regulations of the Eurocode for partially loaded areas [17, 24, 29], as

$$F = \sqrt{F_a F_b}\,, \tag{16}$$

where F_a and F_b account for the lateral and thickness contraction. They are defined as

$$F_a = \min\left[3 \; ; \; \frac{d}{a} \right], \tag{17}$$

and

$$F_b = \min\left[3 \; ; \; \frac{c}{b} \right], \tag{18}$$

see Fig. 1 for the meaning of the letter symbols in Eqs. (17) and (18).

2.2. Serviceability limit states of reinforced concrete hinges for different operating conditions

The aim of the following considerations is to assign a maximum tolerable relative rotation $\Delta\varphi_\ell$ to

every bearable degree of utilization of the normal force, ν. Thereby, $\Delta\varphi_\ell$ corresponds to a serviceability limit state (SLS). A reinforced concrete hinge reaches its serviceability limit if either the steel rebars start to yield or the maximum compressive normal stress of concrete reaches the elastic limit stress $|Ff_c|$, or both occur simultaneously. Bending-induced tensile macrocracking of concrete, however, is accepted, because it reduces the bending stiffness of the neck region and, thus, increases the desired rotational compliance of the concrete hinge.

In order to derive analytical formulae, four different operating conditions of reinforced concrete hinges are analyzed. The five serviceability limit states, illustrated in Fig. 5, represent bounding scenarios for the four operating conditions. The corresponding state variables $\Delta\ell_\ell$, $\Delta\varphi_\ell$, a_c, χ, and ν are listed in Table 1.

2.3. Serviceability limits in case of compression-dominated operation

In this case, the serviceability limits are bounded by the scenarios (a) and (b), illustrated in Fig. 5, see also Table 1. The elastic limit of concrete is always reached at the left edge of the neck. The elastic limit strain is given as

$$\varepsilon_c(z{=}-a/2) = -\frac{|Ff_c|}{E_c}\,. \tag{19}$$

The range of the maximum tolerable relative rotation is obtained as

$$0 \le \Delta\varphi_\ell \le \frac{|Ff_c|}{E_c}\,, \tag{20}$$

see Fig. 5 and Table 1. The corresponding values of $\Delta\ell_\ell$ follow from inserting Eq. (19) into Eq. (3) and solving the resulting expression for $\Delta\ell_\ell$:

$$\Delta\ell_\ell = a\left(\frac{\Delta\varphi_\ell}{2} - \frac{|Ff_c|}{E_c}\right). \tag{21}$$

Compression-dominated operation implies $a_c = a$ and $\chi = 0$, see also Fig. 5 and Table 1. Inserting these values of a_c and χ together with Eq. (21) into Eq. (13) and substituting the obtained expression for N into Eq. (15) delivers

$$\nu = 1 - \frac{\Delta\varphi_\ell}{2}\,\frac{E_c}{|Ff_c|}\,. \tag{22}$$

The sought expression for the maximum tolerable relative rotation as a function of ν follows from solving Eq. (22) for $\Delta\varphi_\ell$ as

$$\Delta\varphi_\ell = 2\,(1-\nu)\,\frac{|Ff_c|}{E_c}\,. \tag{23}$$

Notably, inserting Eq. (20) into Eq. (22) shows that compression-dominated operation is related to $\nu \in [\,0.50\;;\;1.00\,]$, see the corresponding part of the abscissa in Fig. 6.

2.4. Serviceability limits in case of tensile macrocracking up to one half of the width of the neck

In this case, the serviceability limits are bounded by the scenarios (b) and (c), illustrated in Fig. 5, see also Table 1. The compressive elastic limit strain of concrete is always reached at the left edge of the neck, see Eq. (19). The range of the maximum tolerable relative rotation is obtained as

$$\frac{|Ff_c|}{E_c} \le \Delta\varphi_\ell \le 2\,\frac{|Ff_c|}{E_c}\,, \tag{24}$$

see Fig. 5 and Table 1. The corresponding values of $\Delta\ell_\ell$ are given in Eq. (21).

Tensile macrocracking up to one half of the width of the neck implies $a/2 \le a_c < a$ and $\chi = 0$, see Fig. 5 and Table 1. The expression for a_c as a function of $\Delta\ell_\ell$ and $\Delta\varphi_\ell$ is obtained as follows: The value of z at the zero position of the strain is obtained by setting Eq. (3) equal to zero and solving the resulting expression for z. This gives

$$z(\varepsilon{=}0) = -\frac{\Delta\ell_\ell}{\Delta\varphi_\ell}\,. \tag{25}$$

The width of the compressed ligament, a_c, is by $a/2$ larger than $z(\varepsilon{=}0)$, see Fig. 5. Thus, a_c follows as

$$a_c = \frac{a}{2} - \frac{\Delta\ell_\ell}{\Delta\varphi_\ell}\,. \tag{26}$$

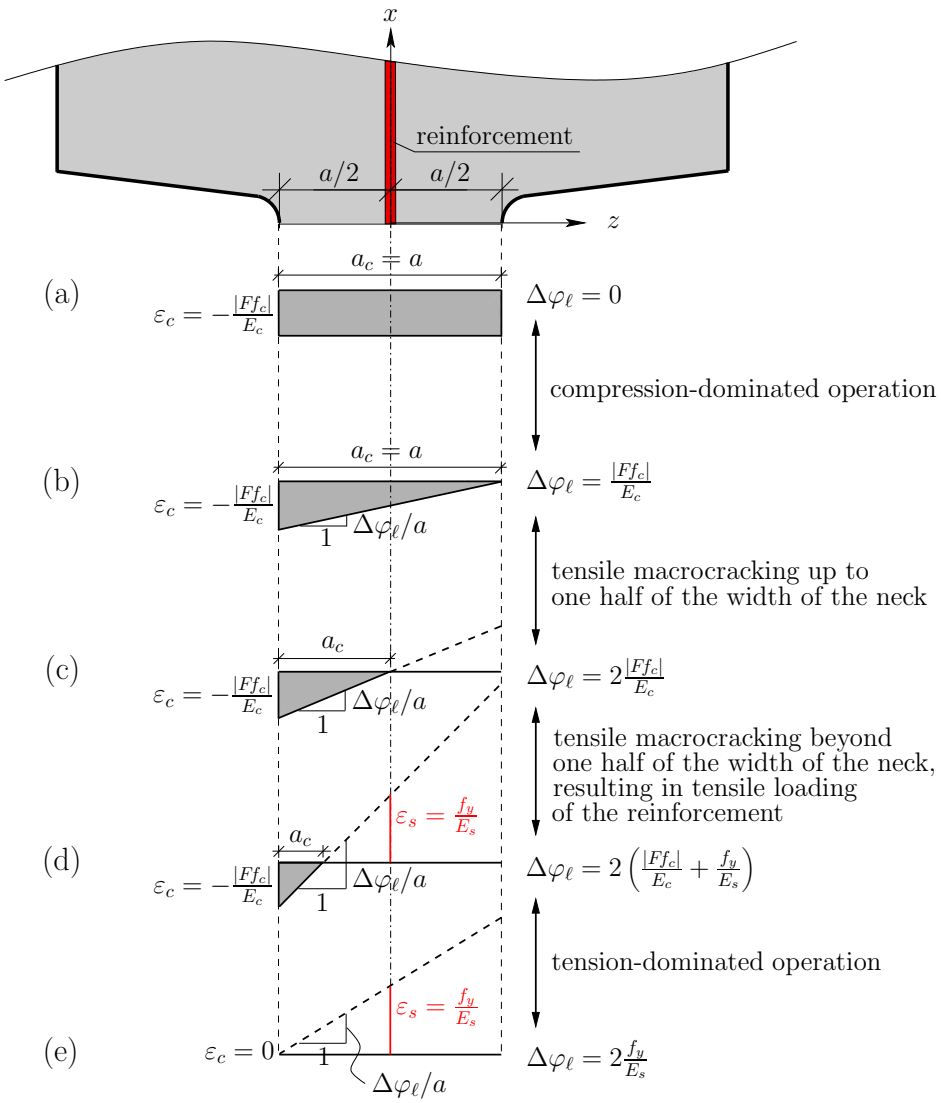

Figure 5: Strain distributions referring to characteristic serviceability limit states of reinforced concrete hinges, see also Eqs. (3) and (4)

Table 1: State variables associated with the serviceability limit states of reinforced concrete hinges illustrated in Fig. 5

SLS	$\Delta\ell_\ell$	$\Delta\varphi_\ell$	a_c	χ	ν
(a)	$-a\,\dfrac{\lvert Ff_c\rvert}{E_c}$	0	a	0	1
(b)	$-\dfrac{a}{2}\,\dfrac{\lvert Ff_c\rvert}{E_c}$	$\dfrac{\lvert Ff_c\rvert}{E_c}$	a	0	$\dfrac{1}{2}$
(c)	0	$2\,\dfrac{\lvert Ff_c\rvert}{E_c}$	$\dfrac{a}{2}$	0	$\dfrac{1}{4}$
(d)	$a\,\dfrac{f_y}{E_s}$	$2\left(\dfrac{\lvert Ff_c\rvert}{E_c}+\dfrac{f_y}{E_s}\right)$	$\dfrac{a}{2}-\dfrac{\Delta\ell_\ell}{\Delta\varphi_\ell}$	1	Eq. (32)
(e)	$a\,\dfrac{f_y}{E_s}$	$2\,\dfrac{f_y}{E_s}$	0	1	$-\dfrac{\rho\,f_y}{\lvert Ff_c\rvert}$

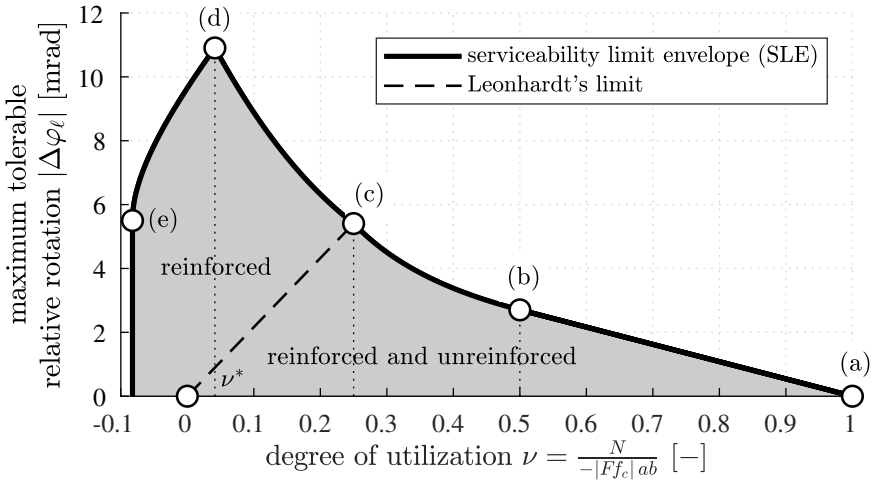

Figure 6: Maximum tolerable relative rotation as a function of the degree of utilization of the normal force, for both reinforced and unreinforced concrete hinges; evaluation of Eqs. (23), (28), (31), (37), and (45) for $|Ff_c| = 100\,\text{MPa}$, $E_c = 37\,\text{GPa}$, $f_y = 550\,\text{MPa}$, $E_s = 200\,\text{GPa}$, and $\rho = 1.5\%$ ($\nu < 0$ refers to the theoretical case of a tensile normal force transmitted across the neck)

Inserting $\chi = 0$ and Eq. (26) into Eq. (13), specializing the resulting expression for $\Delta\ell_\ell$ according to Eq. (21), and substituting the obtained expression for N into Eq. (15) delivers

$$\nu = \frac{1}{2\,\Delta\varphi_\ell}\,\frac{|Ff_c|}{E_c}\,. \tag{27}$$

The sought expression for the maximum tolerable relative rotation as a function of ν follows from solving Eq. (27) for $\Delta\varphi_\ell$ as

$$\Delta\varphi_\ell = \frac{1}{2\,\nu}\,\frac{|Ff_c|}{E_c}\,. \tag{28}$$

Notably, inserting Eq. (24) into Eq. (27) shows that tensile macrocracking up to one half of the width of the neck is related to $\nu \in [\,0.25\;;\;0.50\,]$, see the corresponding part of the abscissa in Fig. 6.

2.5. Serviceability limits in case of tensile macrocracking beyond one half of the width of the neck, resulting in tensile loading of the reinforcement

In this case, the serviceability limits are bounded by the scenarios (c) and (d), illustrated in Fig. 5, see also Table 1. The elastic limit of the compressive strain of concrete is always reached at the left edge of the neck, see Eq. (19). The range of the maximum tolerable relative rotation is obtained as

$$2\,\frac{|Ff_c|}{E_c} \le \Delta\varphi_\ell \le 2\left(\frac{|Ff_c|}{E_c} + \frac{f_y}{E_s}\right), \tag{29}$$

see Fig. 5 and Table 1. The corresponding values of $\Delta\ell_\ell$ are given in Eq. (21).

Tensile macrocracking beyond one half of the width of the neck refers to $0 \le a_c \le a/2$ and $\chi = 1$, see Fig. 5 and Table 1. Inserting $\chi = 1$ and a_c according to Eq. (26) into Eq. (13), specializing the resulting expression for $\Delta\ell_\ell$ according to Eq. (21), and substituting the obtained expression for N into Eq. (15) delivers

$$\nu = \frac{1}{2\,\Delta\varphi_\ell}\,\frac{|Ff_c|}{E_c} + \left(\frac{|Ff_c|}{E_c} - \frac{\Delta\varphi_\ell}{2}\right)\frac{\rho\,E_s}{|Ff_c|}\,. \tag{30}$$

The sought expression for the maximum tolerable relative rotation as a function of ν follows from solving Eq. (30) for $\Delta\varphi_\ell$ as

$$\begin{aligned}\Delta\varphi_\ell \;=\; & \frac{|Ff_c|}{\rho\,E_s}\Bigg[\left(\frac{\rho\,E_s}{E_c} - \nu\right) \\ & + \sqrt{\left(\frac{\rho\,E_s}{E_c} - \nu\right)^2 + \frac{\rho\,E_s}{E_c}}\Bigg]. \end{aligned}\tag{31}$$

Notably, inserting Eq. (29) into Eq. (30) shows that tensile macrocracking beyond one half of the width of the neck refers to $\nu \in [\,\nu^*\;;\;0.25\,]$, with

$$\nu^* = \frac{1}{4}\left(\frac{f_y}{|Ff_c|}\,\frac{E_c}{E_s} + 1\right)^{-1} - \frac{\rho\,f_y}{|Ff_c|}\,, \tag{32}$$

see the corresponding part of the abscissa in Fig. 6.

2.6. Serviceability limits in case of tension-dominated operation

In this case, the serviceability limits are bounded by the scenarios (d) and (e) illustrated in Fig. 5, see also Table 1. The elastic limit of steel is always reached by prescribing that the strain of the rebars is equal to the yield strain

$$\varepsilon(z{=}0) = \frac{f_y}{E_s}\,. \tag{33}$$

The range of the maximum tolerable relative rotation is obtained as

$$2\left(\frac{|Ff_c|}{E_c} + \frac{f_y}{E_s}\right) \ge \Delta\varphi_\ell \ge 2\,\frac{f_y}{E_s}\,, \tag{34}$$

see Fig. 5 and Table 1. The corresponding value of $\Delta\ell_\ell$ follows from inserting Eq. (33) into Eq. (3) and solving the resulting expression for $\Delta\ell_\ell$. It is obtained as

$$\Delta\ell_\ell = a\,\frac{f_y}{E_s}\,. \tag{35}$$

Tension-dominated operation refers to $0 \le a_c < a/2$ and $\chi = 1$, see Fig. 5 and Table 1. Inserting $\chi = 1$ and a_c according to Eq. (26) into Eq. (13), specializing the resulting expression for $\Delta\ell_\ell$ according to Eq. (35), and substituting the obtained expression for N into Eq. (15) delivers

$$\nu = \frac{E_c}{|Ff_c|}\,\frac{1}{2\,\Delta\varphi_\ell}\left(\frac{\Delta\varphi_\ell}{2} - \frac{f_y}{E_s}\right)^2 - \frac{\rho\,f_y}{|Ff_c|}\,. \tag{36}$$

The sought expression for the maximum tolerable relative rotation as a function of ν follows from solving Eq. (36) for $\Delta\varphi_\ell$ as

$$\Delta\varphi_\ell = \frac{2}{E_c}\left\{ f_y \left(\frac{E_c}{E_s} + 2\rho \right) + 2|Ff_c|\,\nu \right. \qquad (37)$$

$$\left. + \sqrt{\left[f_y \left(\frac{E_c}{E_s} + 2\rho \right) + 2|Ff_c|\,\nu \right]^2 - \left(f_y \frac{E_c}{E_s} \right)^2} \right\}.$$

Notably, inserting Eq. (34) into Eq. (36) shows that tension-dominated operation of a reinforced concrete hinge is related to $\nu \in [\, -\rho\, f_y/|Ff_c| \;;\; \nu^* \,]$, with ν^* according to Eq. (32), see the corresponding part of the abscissa in Fig. 6.

2.7. Position stability of reinforced and unreinforced concrete hinges

The rebars contribute to the position stability of reinforced concrete hinges. This contribution is essential, provided that the reinforcement is subjected to tension, see the operating conditions "tensile macrocracking beyond one half of the width of the neck, resulting in tensile loading of the reinforcement" and "tension-dominated operation". Because the crack is larger than $a/2$, the compressed ligament is smaller than one half of the width of the neck, i.e.

$$a_c < \frac{a}{2}\,. \qquad (38)$$

For *un*reinforced concrete hinges pronounced macrocracking according to Eq. (38) is associated with the risk of loss of position stability. Thus, according to Leonhardt and Reimann [6] a safe operation of unreinforced concrete hinges requires that the compressed ligament is larger than or equal to one half of the width of the neck: $a_c \geq a/2$. This condition is satisfied in case of " compression-dominated operation " and "tensile macrocracking up to one half of the width of the neck". Thus, the developments described in Subsections 2.3 and 2.4 are also applicable to unreinforced concrete hinges. The limiting case,

$$a_c = \frac{a}{2}\,, \qquad (39)$$

defines another serviceability limit of *un*reinforced concrete hinges. The axial strain vanishes in the plane of symmetry, i.e.

$$\varepsilon(z{=}0) = 0\,. \qquad (40)$$

Inserting Eq. (40) into Eq. (3) yields

$$\Delta\ell_\ell = 0\,. \qquad (41)$$

The axial strain is compressive at the left edge of the neck:

$$-\frac{|Ff_c|}{E_c} \leq \varepsilon_c(z{=}-a/2) \leq 0\,. \qquad (42)$$

Substituting Eqs. (41) and (42) into Eq. (3) and solving the resulting expression for $\Delta\varphi_\ell$ yields

$$0 \leq \Delta\varphi_\ell \leq 2\frac{|Ff_c|}{E_c}\,. \qquad (43)$$

Inserting Eqs. (39) and (41) together with $\rho = 0$ into Eq. (13) and substituting the obtained expression for N into Eq. (15) delivers

$$\nu = \frac{1}{8}\,\frac{E_c}{|Ff_c|}\,\Delta\varphi_\ell\,. \qquad (44)$$

The sought expression for the maximum tolerable relative rotation as a function of ν follows from solving Eq. (44) for $\Delta\varphi_\ell$ as

$$\Delta\varphi_\ell = 8\,\nu\,\frac{|Ff_c|}{E_c}\,, \qquad (45)$$

see the dashed line in Fig. 6. Notably, inserting Eq. (43) into Eq. (44) shows that the described serviceability limit of *un*reinforced concrete hinges is related to $\nu \in [\,0.00\;;\;0.25\,]$, see Fig. 6.

3. Assessment of the theoretical investigation by means of experimental data

In order to assess the usefulness of the theoretical investigation, its results are applied to the analysis of experiments on reinforced concrete hinges. The experimental data refer to two different test protocols, see Table 2 for details.

One series of analyzed tests refers to eccentric compression. The eccentricity of the normal force N is denoted as e. Hence, the bending moment reads as

$$M = N\,e\,. \tag{46}$$

One set of tests was carried out by Schlappal et al., see [12] for the detailed experimental procedures. Moreover, results from new experiments, following the test protocol described in [12], are presented in Subsection 3.1.

The experiments of the other series of analyzed tests are organized in two steps. At first, the reinforced concrete hinges are subjected to a specific compressive normal force N which is kept constant thereafter. Then, the hinges are subjected to bending. Cyclic bending was used by the present research team, see Subsection 3.2 for new test results and [32] for the detailed experimental procedures. Monotonously increasing bending was used by Base [9], as well as by Hordijk and Gijsbers [11], see Subsection 3.3 and 3.4, respectively.

3.1. Eccentric compression tests

In the bearing capacity tests of reinforced concrete hinges subjected to eccentric compression, carried out by Schlappal et al. [12] and by the present research team, the relative rotations were measured, using eight inductive displacement transducers, see also [12]. Three sets of tests are described in the following, labeled as A1, A2, and A3, see Table 2. Set A1 refers to three nominally identical reinforced concrete hinges, produced with normal-strength concrete and aggregates with a maximum diameter amounting to 16 mm, see [12]. The sets A2 and A3 are newly presented. Set A2 refers to two nominally identical specimens, normal-strength concrete, and maximum aggregate diameters amounting to 8 mm and set A3 to three nominally identical specimens, high-strength concrete, and maximum aggregate diameters amounting to 8 mm.

The recorded data of sets A1, A2, and A3 are shown in Figs. 7 (a), (c), and (e), respectively. The kinks in the graphs refer to short periods of time during which the loading process was stopped and the displacement of the piston of the testing machine was kept constant. During these periods the relative rotations increased and the normal forces decreased. Thus, the kinks refer to the time-dependent behavior of the concrete hinges.

Serviceability limit diagrams for the tested concrete hinges are computed based on the theoretical investigation in Section 2, see Figs. 7 (b), (d), and (f). In more detail, the Eqs. (23), (28), (31), (37), and (45) are evaluated based on the geometric dimensions of the tested concrete hinges and the properties of the concrete and the rebars used, see Table 2. Graphs, illustrating the test data, are added to the diagrams showing the serviceability limit envelope (SLE). In the present context of eccentric compression tests, M is directly proportional to N, see Eq. (46). Thus, the relation between $\Delta\varphi$ and M is affine to the relation between $\Delta\varphi$ and ν, compare Figs. 7 (a), (c), and (e) with Figs. 7 (b), (d), and (f).

The points at which the graphs of the experimental data intersect the graphs of the serviceability limit envelope, allow for the identification of pairs of serviceability limit state values, consisting of a specific normal force and relative rotation, see the circles in Figs. 7 (b), (d), and (f). Marking these points in the graphs of the experimental data, see Figs. 7 (a), (c), and (e), allows for identifying serviceability limit states (SLS) of the tested concrete hinges. Up to the identified serviceability limits the concrete hinges behave in a moderately nonlinear fashion, while significant nonlinearities follow beyond the serviceability limits, see Figs. 7 (a), (c), and (e). This underlines that the theoretical investigation in Section 2 describes serviceability limits of reinforced concrete hinges in an acceptable fashion for engineering applications.

3.2. Cyclic bending at a constant normal force

In the present research, reinforced concrete hinges have been subjected to cyclic bending at a constant normal force. In the following, the tests are described and the test results are presented. The specimens were first subjected to compressive line loads, using a steel frame and four hydraulic jacks of the manufacturer Hainzl. Keeping the normal force constant, the concrete hinges were subjected to bending using four smaller hydraulic cylinders of the type Enerpac SLP

Table 2: Experimental data taken from Schlappal et al. [12] (A1), Base [9] (Base), and Hordijk and Gijsbers [11] (HG); the data sets A2, A3, B1, B2, and B3 represent original experimental contributions

Type	$\|N\|$ [kN]	e [mm]	ν [-]	a [mm]	b [mm]	c [mm]	d [mm]	F [-]	$\|f_c\|$ [MPa]	E_c [GPa]	f_y [MPa]	E_s [GPa]	ρ [%]	Source
A1	$\|M\|/e$	25	-	75	300	400	250	2.00	46.88	34.8	550	200	1.30	[12]
A2	$\|M\|/e$	25	-	75	300	400	250	2.00	45.22	32.8	550	200	1.30	oc[1]
A3	$\|M\|/e$	25	-	75	300	400	250	2.00	75.42	39.0	550	200	1.30	oc[1]
B1	1300	M/N	0.127	150	520	820	500	2.18	60.42	35.0*	550	200	0.87	oc[1]
B1	2600	M/N	0.254	150	520	820	500	2.18	60.42	35.0*	550	200	0.87	oc[1]
B1	4500	M/N	0.439	150	520	820	500	2.18	60.42	35.0*	550	200	0.87	oc[1]
B2	1300	M/N	0.177	100	620	820	500	1.99	59.33	35.0*	550	200	1.09	oc[1]
B2	2600	M/N	0.355	100	620	820	500	1.99	59.33	35.0*	550	200	1.09	oc[1]
B2	4500	M/N	0.614	100	620	820	500	1.99	59.33	35.0*	550	200	1.09	oc[1]
B3	2600	M/N	0.195	100	620	820	500	1.99	107.8	43.8	550	200	1.09	oc[1]
B3	3500	M/N	0.263	100	620	820	500	1.99	107.8	43.8	550	200	1.09	oc[1]
B3	5400	M/N	0.263	100	620	820	500	1.99	107.8	43.8	550	200	1.09	oc[1]
Base	750	M/N	0.247	197	152	152	610	1.73	58.59	35.0*	550*	200*	0.85	[9]
HG	100	M/N	0.015	158	500	500	350	1.49	58.25	32.4	240	200*	0.51	[11]
HG	450	M/N	0.066	158	500	500	350	1.49	58.25	32.4	240	200*	0.51	[11]
HG	800	M/N	0.117	158	500	500	350	1.49	58.25	32.4	240	200*	0.51	[11]
HG	1150	M/N	0.168	158	500	500	350	1.49	58.25	32.4	240	200*	0.51	[11]
HG	1500	M/N	0.219	158	500	500	350	1.49	58.25	32.4	240	200*	0.51	[11]
HG	2200	M/N	0.321	158	500	500	350	1.49	58.25	32.4	240	200*	0.51	[11]

[1] original contribution to the present manuscript

* estimated value

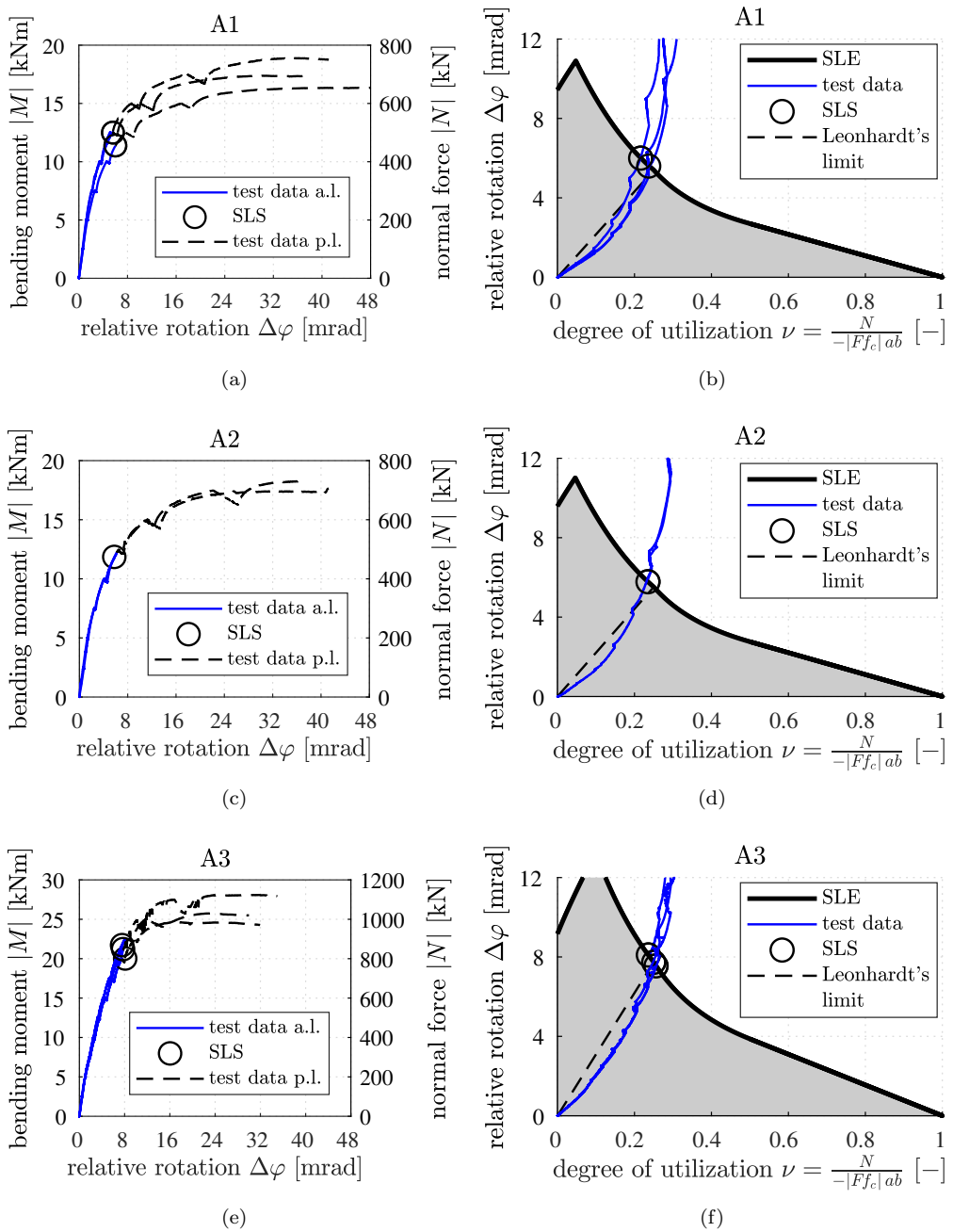

SLE = serviceability limit envelope; SLS = serviceability limit state
a.l. = ante limitem (= before SLS); p.l. = post limitem (= after SLS)

Figure 7: Analysis of eccentric compression tests on reinforced concrete hinges: (a), (c), and (e) show experimental data; (b), (d), and (f) refer to the identification of serviceability limits based on the theoretical investigation in Section 2; see also Table 2 for data sets A1, A2, and A3

602. The tests were carried out, using a hand-guided control, see [32] for the detailed experimental procedures. Inductive Displacement Transducers were attached to the specimens in each of the corner regions. They measured changes of the notch mouth opening displacements of the lateral notches, see Fig. 8. The obtained readings were used to quantify the relative rotation.

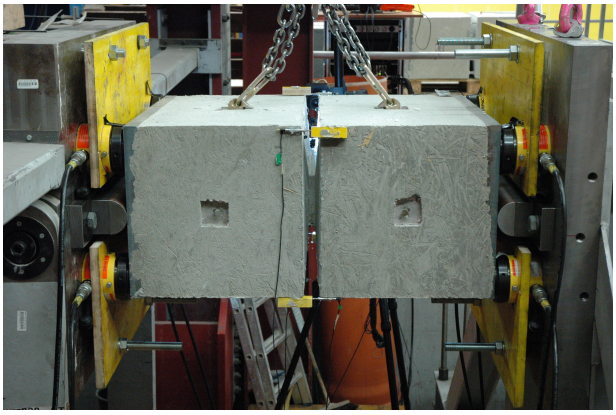

Figure 8: Structural testing of concrete hinges: Inductive Displacement Transducers were mounted to each corner of the concrete hinges; normal forces N were imposed in form of centric line loads; bending moments M were imposed, using four hydraulic cylinders

Three types of specimens were investigated, labeled as B1, B2, and B3, see Table 2. Specimens B1 were produced with an a/d-ratio amounting to 0.3 and with a normal-strength concrete, specimens B2 with $a/d = 0.2$ and normal-strength concrete, and specimens B3 with $a/d = 0.2$ and high-strength concrete. In all of these three cases, three pairs of crossing steel rebars, with a diameter of 1.2 cm, were running across the neck.

Three nominally identical reinforced concrete hinges were produced and tested for each one of the three specimen types, resulting in a total of nine specimens, see Table 2. As for the three specimens of type B1, the normal forces amounted to $-1300\,\mathrm{kN}$, $-2600\,\mathrm{kN}$, and $-4500\,\mathrm{kN}$, respectively. The same values of the normal forces were used for the tests on specimens B2. As for specimens B3, these forces amounted to $-2600\,\mathrm{kN}$, $-3500\,\mathrm{kN}$, and $-5400\,\mathrm{kN}$, respectively. These forces were selected in order to test the concrete hinges in markedly different regions of estimated N,M-interaction diagrams, see Fig. 5.25 of [32]. Subsequently, relative rotations were imposed in a cyclic fashion in the range of $\pm 3\,\mathrm{mrad}$. After several cycles, positive relative rotations were imposed with increasing amplitudes, followed by the removal of the applied bending moment. The maximum relative rotation amounted to $\approx 20\,\mathrm{mrad}$. Notably, in the experiments the bearing capacity of the concrete hinges was never reached, see the test results, illustrated in Figs. 9 (a), (b), (c), 10 (a), (b), (c), and 11 (a), (b), (c).

Serviceability limit diagrams for the tested concrete hinges are computed based on Eqs. (23), (28), (31), (37), and (45), specialized for the geometric dimensions of the tested concrete hinges and the properties of the concrete and the rebars used, see Table 2 and Figs. 9 (d), 10 (d), and 11 (d). Graphs illustrating the test data are added to the diagrams showing the serviceability limit envelope. In the tests, carried out with a constant normal force, $\Delta\varphi$ was increased and decreased at a constant value of ν, see Figs. 9 (d), 10 (d), and 11 (d). The three experiments of each specimen type are highlighted in red, green, and blue, respectively.

The points at which the graphs of the experimental data intersect the graphs of the serviceability limit envelope, allow for the identification of pairs of serviceability limit state values consisting of a specific normal force and relative rotation, see the circles in Figs. 9 (d), 10 (d), and 11 (d). Marking these points in the graphs of the experimental data, see Figs. 9 (a), (b), (c), 10 (a), (b), (c), and 11 (a), (b), (c), allows for identifying serviceability limit states of the tested concrete hinges. Up to the identified serviceability limits, the concrete hinges behave in a nonlinear fashion, see Figs. 9 (a), (b), (c), 10 (a), (b), (c), and 11 (a), (b), (c). The nonlinearities mainly refer to progressive tensile macrocracking during loading, closure of such cracks during unloading, re-opening and further propagation of the cracks during subsequent test cycles. Cyclic bending below the serviceability limit induces virtually reversible behavior. Cyclic bending beyond the serviceability limit, however, induces irreversible deformations. This is exemplarily demon-

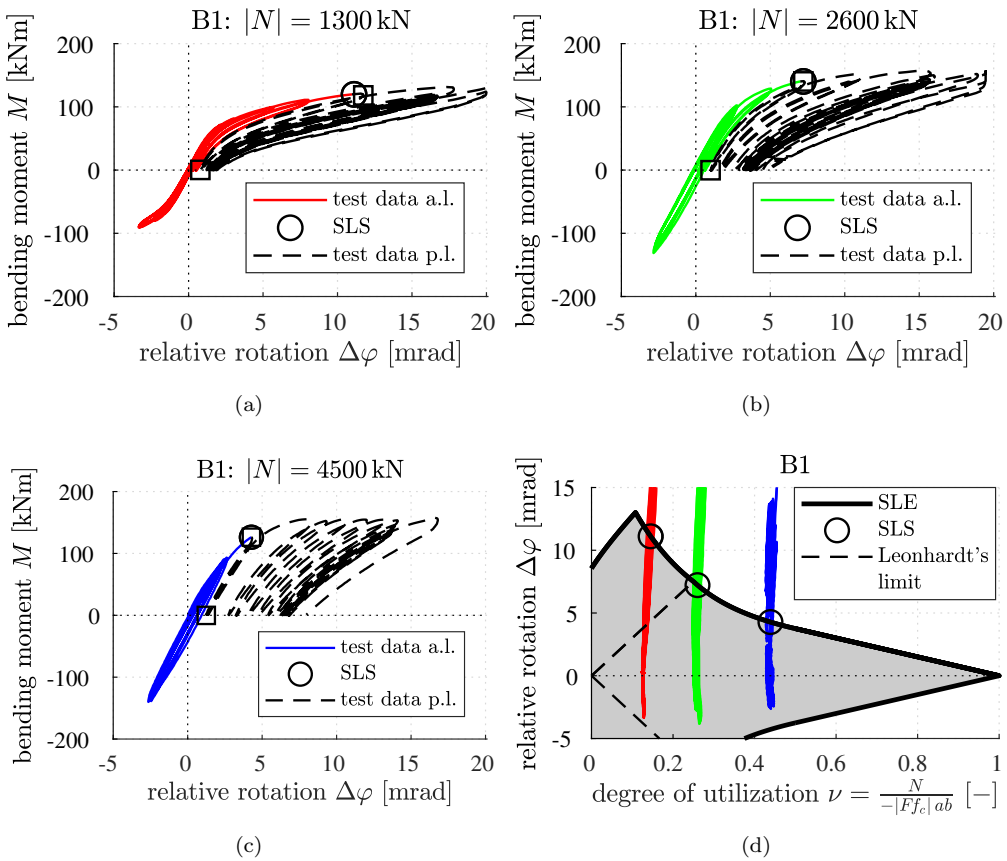

Figure 9: Analysis of tests with cyclic bending, at a constant normal force, on reinforced concrete hinges: (a), (b), and (c) show experimental data; (d) refers to identification of serviceability limits based on the theoretical investigation in Section 2; see also Table 2 for data set B1; the square symbols highlight the specific loading-unloading cycle in which the model-predicted serviceability limit is either reached or slightly exceeded for the first time

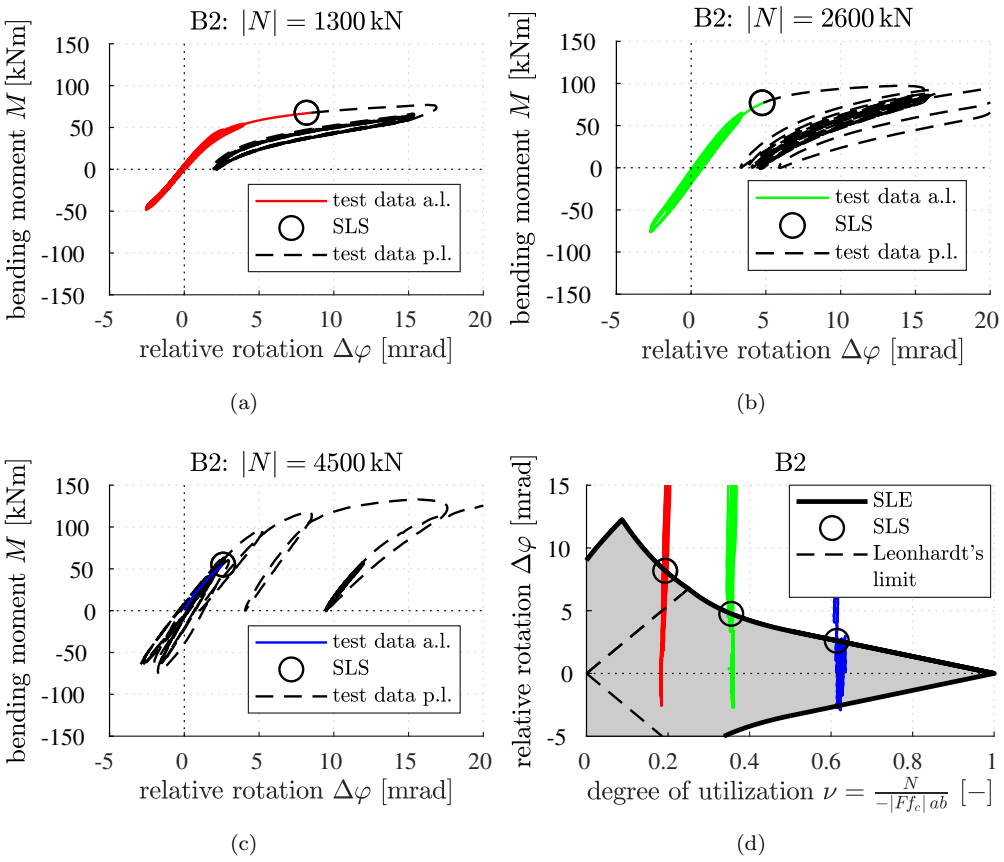

Figure 10: Analysis of tests with cyclic bending, at a constant normal force, on reinforced concrete hinges: (a), (b), and (c) show experimental data; (d) refers to identification of serviceability limits based on the theoretical investigation in Section 2; see also Table 2 for data set B2

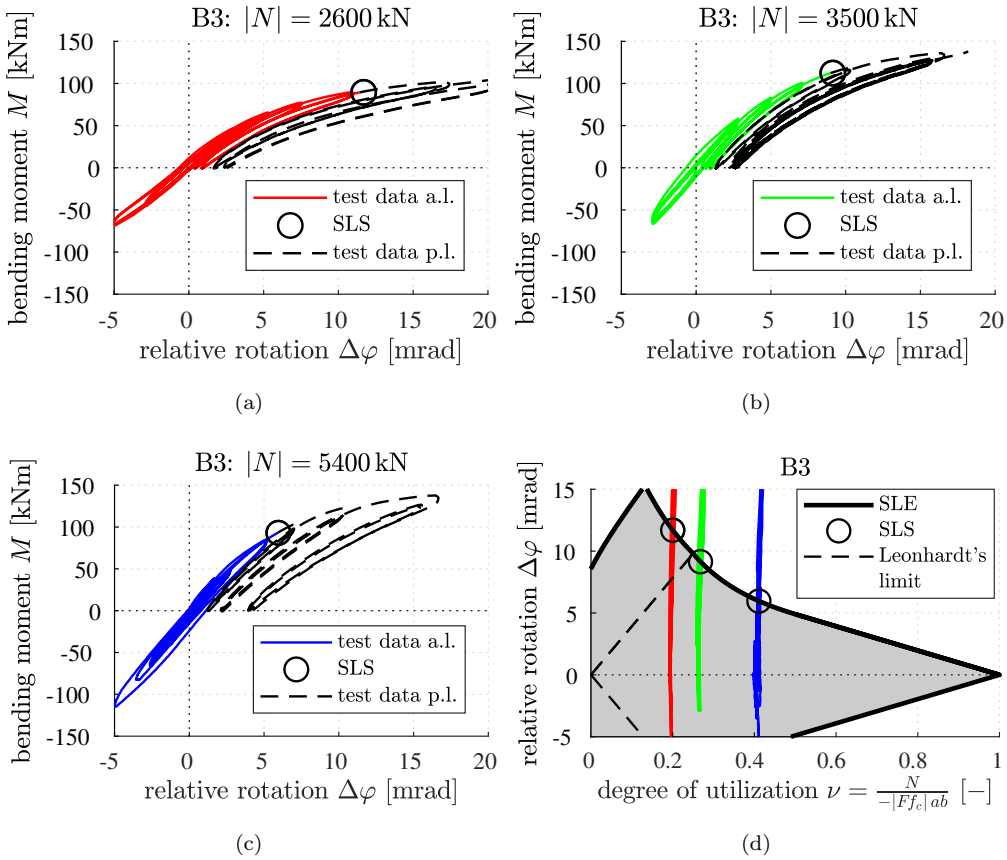

SLE = serviceability limit envelope; SLS = serviceability limit state
a.l. = ante limitem (= before SLS); p.l. = post limitem (= after SLS)

Figure 11: Analysis of tests with cyclic bending, at a constant normal force, on reinforced concrete hinges: (a), (b), and (c) show experimental data; (d) refers to identification of serviceability limits based on the theoretical investigation in Section 2; see also Table 2 for data set B3

strated in Figs. 9 (a), (b), and (c). Squares are used to highlight the maximum of the specific loading-unloading cycle in which the model-predicted serviceability limit is either reached or slightly exceeded for the first time, i.e. that the elastic limit of concrete in compression or the one of steel in tension is exceeded, at least when assessed from the viewpoint of the derived formulae.

One square marks the maximum loading applied during that test cycle. Another square marks the residual relative rotation measured at the end of that test cycle, i.e. after complete unloading to $M = 0\,\mathrm{kNm}$. These residual relative rotations would have further decreased, if sufficient time had been provided for creep recovery. Still, the marked residual relative rotations are small compared to the ones measured at the end of the subsequent test cycles, which were progressing further beyond the serviceability limit. This underlines that the theoretical investigation in Section 2 describes serviceability limits of reinforced concrete hinges in an acceptable fashion for engineering applications.

3.3. Experiments by Base (1962): monotonously increasing bending at a constant normal force

Base [9] subjected a reinforced concrete hinge to monotonously increasing bending at a constant normal force amounting to $-750\,\mathrm{kN}$, see Table 2. The relative rotation was increased monotonously. As for the recorded data, see the squares in Fig. 12 (a). A trendline is fitted to the experimental data in order to illustrate the relation between M and $\Delta\varphi$ in a continuous fashion.

The serviceability limit diagram for the tested concrete hinge is computed based on Eqs. (23), (28), (31), (37), and (45), specialized for the geometric dimensions of the tested concrete hinge and the properties of the concrete and the rebars used, see Table 2 and Fig. 12 (b). The graph illustrating the test data (square symbols) is added to the diagram showing the serviceability limit envelope. The serviceability limit state is identified as explained before, and this point is also marked in the graph of the experimental data, see Fig. 12 (a). It is concluded that the analysis of the tests by Base [9] delivers results similar to those presented in the preceding Subsections.

3.4. Experiments by Hordijk and Gijsbers (1996): monotonously increasing bending at a constant normal force

Hordijk and Gijsbers [11] subjected reinforced concrete hinges to monotonously increasing bending at a constant normal force, see Table 2 for data with the label HG. Six nominally identical reinforced concrete hinges were subjected to a specific normal force, amounting to $-100\,\mathrm{kN}$, $-450\,\mathrm{kN}$, $-800\,\mathrm{kN}$, $-1150\,\mathrm{kN}$, $-1500\,\mathrm{kN}$, and $-2200\,\mathrm{kN}$, respectively. These forces were selected in order to test the concrete hinges in markedly different regions regarding the degree of utilization of the normal force. Subsequently, relative rotations were increased monotonously. The recorded data are shown in Fig. 13 (a).

The serviceability limit diagram for the tested concrete hinge is computed based on Eqs. (23), (28), (31), (37), and (45), specialized for the geometric dimensions of the tested concrete hinges and the properties of the concrete and the rebars used, see Table 2 and Fig. 13 (b). The test data are added to the diagram showing the serviceability limit envelope. The serviceability limit state values are identified as explained before, and these points are marked in the graphs of the experimental data, see Fig. 13 (a). It is concluded that the analysis of the tests by Hordijk and Gijsbers [11] delivers results similar to those described in the preceding Subsections.

4. Verification of serviceability limit states of reinforced concrete hinges in integral bridge construction

The engineering mechanics model developed in Section 2 was shown to be suitable for the description of serviceability limits of reinforced concrete hinges, see Section 3. This provides the motivation for applying the model to verification of serviceability limit states in integral bridge construction.

4.1. Layout of the geometric shape of reinforced concrete hinges

As for the layout of structural dimensions of concrete hinges, the following recommendations are

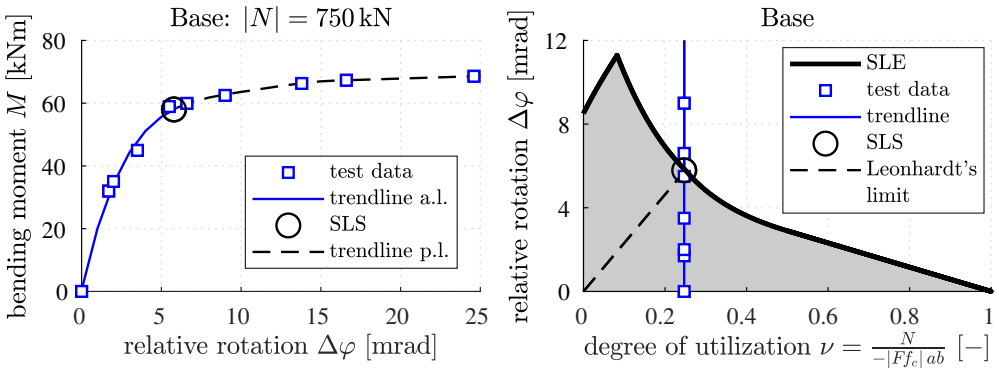

(a) (b)

SLE = serviceability limit envelope; SLS = serviceability limit state
a.l. = ante limitem (= before SLS); p.l. = post limitem (= after SLS)

Figure 12: Analysis of a test with a constant normal force and a monotonously increasing bending moment on reinforced concrete hinges: (a) shows experimental data; (b) refers to identification of serviceability limits based on the theoretical investigation in Section 2; see also Table 2 for data set Base [9]

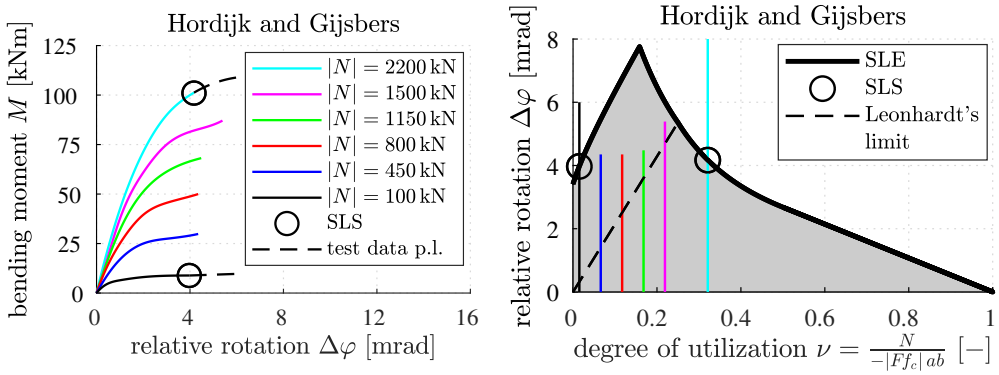

(a) (b)

SLE = serviceability limit envelope; SLS = serviceability limit state
a.l. = ante limitem (= before SLS); p.l. = post limitem (= after SLS)

Figure 13: Analysis of tests at a constant normal force and with a monotonously increasing bending moment on reinforced concrete hinges: (a) shows experimental data; (b) refers to identification of serviceability limits based on the theoretical investigation in Section 2; see also Table 2 for data set HG [11]

adopted from Leonhardt and Reimann [6]

$$a \leq 0.3\,d\,, \tag{47}$$

$$t \leq \begin{cases} 0.2\,a\,, \\ 2\,\mathrm{cm}\,, \end{cases} \tag{48}$$

$$\tan\beta \leq 0.1\,, \tag{49}$$

$$b_R \geq \begin{cases} 0.7\,a\,, \\ 5\,\mathrm{cm}\,, \end{cases} \tag{50}$$

see Fig. 1 for the definition of the letter symbols used. Eqs. (47)-(50) ensure that beneficial *triaxial* compressive stress states are activated in the region of the neck and that undesirable tensile macrocracking of concrete is avoided further away from the neck, see [6, 24] and Fig. 14.

(a) (b)

Figure 14: Concrete hinges at the Viaduto de Gonçalo Cristóvão, built in 1961, in Porto, Portugal: (a) shows the structural subsystem; (b) refers to structural damage that could have been avoided, if the conditions (47)-(50) had been respected

The *monolithic* production of concrete hinges is facilitated provided the throat of the neck is sufficiently large. This is important, because the concrete for the lower part of the concrete hinge must pass through this bottle-neck, and it must be compacted afterwards. This provides the motivation for the recommended limit, i.e. for $a = 0.3\,d$, see (47).

As for the steel rebars, it is recommended to place their cross-over point at the center of the neck, in order to render the mechanical model of Section 2 applicable. As for the transfer of splitting tensile forces and shear forces it is recommended to follow the guidelines of Leonhardt and Reimann [6], see also [33].

4.2. Verification of serviceability limit states

It is recommended to use a two-step procedure, involving the investigation of two bounding scenarios. In step 1, the concrete hinge shall be modeled as a classical hinge without bending stiffness, see Fig 15 (a). The related structural analysis delivers an *upper* bound for the relative rotation and a *lower* bound for the absolute value of the bending moment: $M = 0\,\mathrm{kNm}$. The design of the concrete hinge is based on computed values for the characteristic normal force N_k and the characteristic relative rotation $\Delta\varphi_k$. In step 2, the maximum of the absolute value of the bending moment that can be activated at the designed reinforced concrete hinge is calculated. The characteristic value of this maximum bending moment, $M_{k,max}$, is imposed on the concrete hinge, and the structural analysis is repeated, see Fig 15 (b). This delivers a *lower* bound for the relative rotation and an *upper* bound for the bending moment. Realistic scenarios must fall in between the two analyzed bounds.

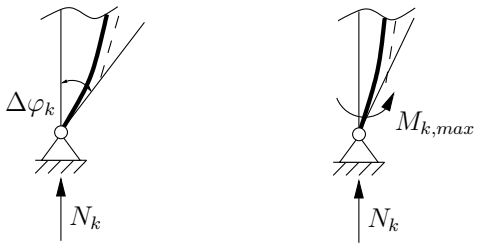

(a) (b)

Figure 15: Bounding scenarios for the design of concrete hinges: (a) classical hinge without bending stiffness; (b) application of the characteristic value of the maximum bending moment $M_{k,max}$ to the concrete hinge

As for step 1, quantification of normal forces and relative rotations is based on combinations of permanent loads (index G), prestressing (index P), and variable loads (index Q). The characteristic values of the normal forces, N_k, are obtained from the regulations of the Eurocode for structural design of bridges

[34, 35, 36]:

$$N_k = \sum_j N_{G,j} + N_P + N_{Q,1} + \sum_{i>1} \psi_{0,i}\, N_{Q,i}\,, \quad (51)$$

where the coefficients $\psi_{0,i} \leq 1$ account for the small probability that several unfavorable non-permanent actions occur simultaneously. As for the related characteristic values of the relative rotations, it is recommended to account for visco-elastic stress-relaxation of concrete, which reduces the bending stresses associated with permanent relative rotations [12]. Following Leonhardt and Reimann [6], this can be accounted for by applying a 50%-reduction to the relative rotations resulting from permanent loads and prestressing, respectively:

$$\begin{aligned} \Delta\varphi_k \;\; = \;\; & \frac{1}{2}\Big[\sum_j \Delta\varphi_{G,j} + \Delta\varphi_P\Big] + \Delta\varphi_{Q,1} \\ & + \sum_{i>1} \psi_{0,i}\, \Delta\varphi_{Q,i}\,. \end{aligned} \quad (52)$$

Because creep and macrocracking of concrete hinges are coupled phenomena [12], stress relaxation results also in a progressive reduction of crack opening displacements. This is beneficial to the long-term behavior of concrete hinges.

As for the layout of reinforced concrete hinges, the design engineer selects a strength class both for the concrete (f_{ck}, E_{cm}) and the steel rebars (f_{yk}, E_{sm}), see Table 3. In the context of the underlying semi-probabilistic safety concept, *characteristic* strength and stiffness values are relevant [17, 37]. In addition, the geometric dimensions of the concrete hinge (a, b, c, d) and the cross-sectional area A_s of the reinforcement running across the neck are chosen, see Fig. 1. These choices allow for quantifying the reinforcement ratio ρ according to Eq. (14), the triaxial-to-uniaxial compressive strength ratio F according to Eq. (16), and the characteristic degree of utilization ν_k according to Eq. (15). A customized serviceability limit envelope is determined based on the Eqs. (23), (28), (31), and (37). All possible combinations of values of ν_k and $|\Delta\varphi_k|$ are inserted into the diagram containing the serviceability limit envelope. An acceptable layout is found, if all combinations of ν_k and $|\Delta\varphi_k|$ are within the serviceability limit envelope.

As for step 2, the maximum of the absolute value of the bending moment that can be activated at the designed reinforced concrete hinge is determined, following the mechanical model in Section 2. The largest bending moment is activated under the operating condition "tensile macrocracking up to one half of the width of the neck", which is the typical service condition. It is expressed as the normal force multiplied by its eccentricity relative to the plane of symmetry:

$$M = \left| N \left(\frac{a}{2} - \frac{a_c}{3} \right) \right| . \quad (53)$$

The maximum value of M can be calculated by specializing Eq. (53) for Eqs. (26), (21), (28), and (15), followed by the solution of an extreme value problem. This delivers

$$M_{max} = \frac{3}{32}\, |F f_c| a^2 b\,. \quad (54)$$

As for quantification of the *characteristic* value of the maximum bending moment, f_c in Eq. (54) must be replaced by an *upper* quantile of the uniaxial compressive strength. Notably, the *lower* quantile f_{ck} is standardly set equal to the mean value of the strength *minus* 8 MPa, see [17, 37]. The value 8 MPa is equal to $1.645\,\sigma_s$, where 1.645 refers to the 5% fractile of a Gaussian strength distribution, and σ_s to the corresponding standard deviation. Based on many experiments, is was found that $\sigma_s \approx 5$ MPa nearly independent of the strength class of concrete [38]. Assuming a symmetric probability distribution function, the *upper* quantile is set equal to the mean value of the strength *plus* 8 MPa. This is equal to $f_{ck} + 16$ MPa, see [18] for a similar approach. One may use a different value than the empirical number 16 MPa, in particular, provided that data regarding the statistical distribution of the strength of a specific concrete are available. Thus, the characteristic value of the maximum bending moment follows as

$$M_{k,max} = \frac{3}{32}\, F \Big(|f_{ck}| + 16\,\mathrm{MPa} \Big)\, a^2 b\,. \quad (55)$$

This bending moment is imposed at the concrete hinge as the basis for the design of the adjacent parts of the reinforced concrete structure.

Table 3: Step-by-step design procedure for verification of serviceability limit states of reinforced concrete hinges

A. Model the concrete hinge as a classical hinge without bending stiffness; analyze all load cases

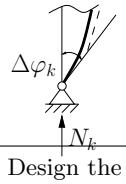

$$N_k = \sum_j N_{G,j} + N_P + N_{Q,1} + \sum_{i>1} \psi_{0,i}\, N_{Q,i}$$

$$\Delta\varphi_k = \frac{1}{2}\left[\sum_j \Delta\varphi_{G,j} + \Delta\varphi_P\right] + \Delta\varphi_{Q,1} + \sum_{i>1} \psi_{0,i}\, \Delta\varphi_{Q,i}$$

B. Design the concrete hinge

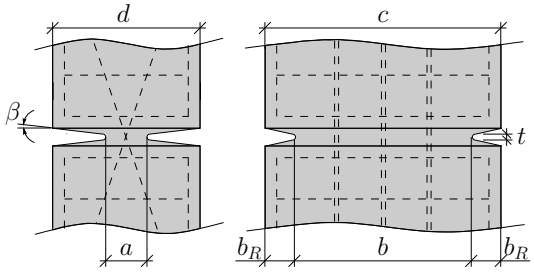

1. Select the concrete: f_{ck}, E_{cm}
2. Select the steel rebars: f_{yk}, E_{sm}
3. Choose geometric dimensions: a, b, c, d
   $a \le 0.3\,d\,,\ t \le \begin{cases} 0.2\,a\,, \\ 2\,\mathrm{cm}\,, \end{cases}\quad \tan\beta \le 0.1\,,\ b_R \ge \begin{cases} 0.7\,a\,, \\ 5\,\mathrm{cm}\,. \end{cases}$
4. Choose the cross-sectional area of reinforcement: A_s
5. Quantify the reinforcement ratio: $\rho = \dfrac{A_s}{ab}$
6. Quantify the triaxial-to-uniaxial compressive strength ratio: $F = \sqrt{F_a F_b}\,,$
   $F_a = \min\left[3\ ;\ \dfrac{d}{a}\right], \quad F_b = \min\left[3\ ;\ \dfrac{c}{b}\right].$
7. The following condition needs to be satisfied: $\displaystyle\sum_j \frac{N_{G,j}}{-|Ff_{ck}|\,ab} \le 0.45$
8. Quantify the degrees of utilization: $\nu_k = \dfrac{N_k}{-|Ff_{ck}|\,ab}$

C. Determine the serviceability limit envelope

1. $\Delta\varphi_{\ell k} = 2\,(1-\nu_k)\,\dfrac{|Ff_{ck}|}{E_{cm}} \quad \nu_k \in [\,0.50\ ;\ 1.00\,]$

2. $\Delta\varphi_{\ell k} = \dfrac{1}{2\,\nu_k}\,\dfrac{|Ff_{ck}|}{E_{cm}} \quad \nu_k \in [\,0.25\ ;\ 0.50\,]$

3. $\Delta\varphi_{\ell k} = \dfrac{|Ff_{ck}|}{\rho\,E_{sm}}\left[\left(\dfrac{\rho\,E_{sm}}{E_{cm}} - \nu_k\right) + \sqrt{\left(\dfrac{\rho\,E_{sm}}{E_{cm}} - \nu_k\right)^2 + \dfrac{\rho\,E_{sm}}{E_{cm}}}\right] \quad \nu_k \in [\,\nu_k^*\ ;\ 0.25\,]$

4. $\Delta\varphi_{\ell k} = \dfrac{2}{E_{cm}}\left\{f_{yk}\left(\dfrac{E_{cm}}{E_{sm}} + 2\,\rho\right) + 2\,|Ff_{ck}|\,\nu_k + \sqrt{\left[f_{yk}\left(\dfrac{E_{cm}}{E_{sm}} + 2\,\rho\right) + 2\,|Ff_{ck}|\,\nu_k\right]^2 - \left(f_{yk}\,\dfrac{E_{cm}}{E_{sm}}\right)^2}\right\}$

   $\nu_k \in \left[-\dfrac{\rho\,f_{yk}}{|Ff_{ck}|}\ ;\ \nu_k^*\right] \quad \nu_k^* = \dfrac{1}{4}\left(\dfrac{f_{yk}}{|Ff_{ck}|}\,\dfrac{E_{cm}}{E_{sm}} + 1\right)^{-1} - \dfrac{\rho\,f_{yk}}{|Ff_{ck}|}$

D. All combinations of ν_k and $|\Delta\varphi_k|$ need to be within the serviceability limit envelope

E. Apply the characteristic value of the maximum bending moment to the concrete hinge; re-analyze all load cases

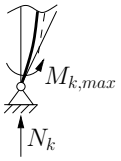

$$M_{k,max} = \frac{3}{32}\,F\Big(|f_{ck}| + 16\,\mathrm{MPa}\Big)\,a^2 b$$

4.3. Exemplary application to the existing Huyck-bridge

The Huyck-bridge [30, 39] is a post-tensioned reinforced concrete frame with a span of 43 m, which was built in the years 2013/14, see Fig. 16. The two abutments are connected to the frame bridge structure by three reinforced concrete hinges each, see Fig. 17 (a). There are two types of concrete hinges, labeled CH1 and CH2. They differ in the depths of the necks and, thus, in the cross sectional area. A detail of one concrete hinge is shown in Fig. 17 (b). As for their material and geometric properties, see Table 4. The concrete hinges were reinforced such that they can transfer shear forces in the context of a quite moderate normal force [40, 6].

Because no design recommendations for verification of serviceability limit states of reinforced concrete hinges were available in 2013, the design was limited to verification of ultimate limit states according to the guidelines of Marx and Schacht [24, 25]. This provides the motivation for *a posteriori* verification of serviceability limit states following the flowchart of Table 3.

In order to calculate normal forces and relative rotations, the concrete hinges were modeled as classical hinges without bending stiffness [39, 40]. Structural analysis was carried out according to the regulations of the Eurocode for structural design of bridges [34, 35, 36]. The analyzed load cases included permanent and variable actions, see Table 5. Permanent actions result from (1) dead load, (2) prestressing, (3) lateral soil pressure, (4) creep and shrinkage of concrete, and (5) potential soil settlements underneath the abutments. Variable actions result from traffic loads and temperature changes. As for traffic loads according to the load model 1 of Eurocode 1 [36], (6) vertical actions, (7) horizontal actions resulting from braking/accelerating, and (8) the activated lateral soil pressure are taken into account. Finally, traffic loads according to the load model 3 of Eurocode 1 [36], resulting from transportation of heavy goods and temperature changes are accounted for, see items (9) and (10), respectively. As for the soil settlement and all variable actions, two different unfavorable cases were analyzed. They are labeled as A and B.

Characteristic values of the normal forces and the relative rotations are computed according to Eqs. (51) and (52). All combinations of load cases, from a practical viewpoint, are considered. In order to increase the safety level, the coefficients $\psi_{0,i}$ in Eqs. (51) and (52) are set equal to one, because there is no experience with verification of serviceability limit states of reinforced concrete hinges, and because relative rotations resulting from permanent actions and prestressing, respectively, are anyway already subjected to a 50%-reduction, see Eq. (52). Finally, the computed N_k-values are translated into characteristic degrees of utilization ν_k according to Eq. (15). All computed pairs of values of ν_k and $|\Delta\varphi_k|$ are labeled as circles in dimensionless design diagrams, see Fig. 18.

As for verification of serviceability limit states, serviceability limit envelopes are added to the dimensionless design diagrams, see Fig. 18. They are computed based on the Eqs. (23), (28), (31), and (37) and on the material and geometric properties of the concrete hinges, see Table 4. All combinations of characteristic values of ν_k and $|\Delta\varphi_k|$ turn out to be *within* the serviceability limit envelopes. Thus, the serviceability limit states are verified *a posteriori*.

It is remarkable that some of the data points in Fig. 18 are above the dashed line, representing the limiting case characterized by the restriction of tensile macrocracking of concrete to one half of the smallest cross-section of the concrete hinges, see Subsection 2.7. One could speculate that this is a result of setting all coefficients $\psi_{0,i}$ in Eqs. (51) and (52) equal to one. However, some data points would remain above the dashed line in Fig. 18, even if all coefficients $\psi_{0,i}$ in Eqs. (51) and (52) were set equal to zero, e.g. the pair of values ν_k and $|\Delta\varphi_k|$ referring to the combination of load cases (1) dead load, (2) prestress, (3) lateral soil pressure, (4) creep and shrinkage of concrete, (5) soil settlement of type B, and (10) temperature change of type B, see the squares in Fig. 18. It is concluded that the compressed ligament of the concrete hinges will eventually be smaller than one half of the width of the neck, even during regular service of the Huyck-bridge. This situation is acceptable, because of the stabilizing role of the reinforcement, which was explicitly accounted for in

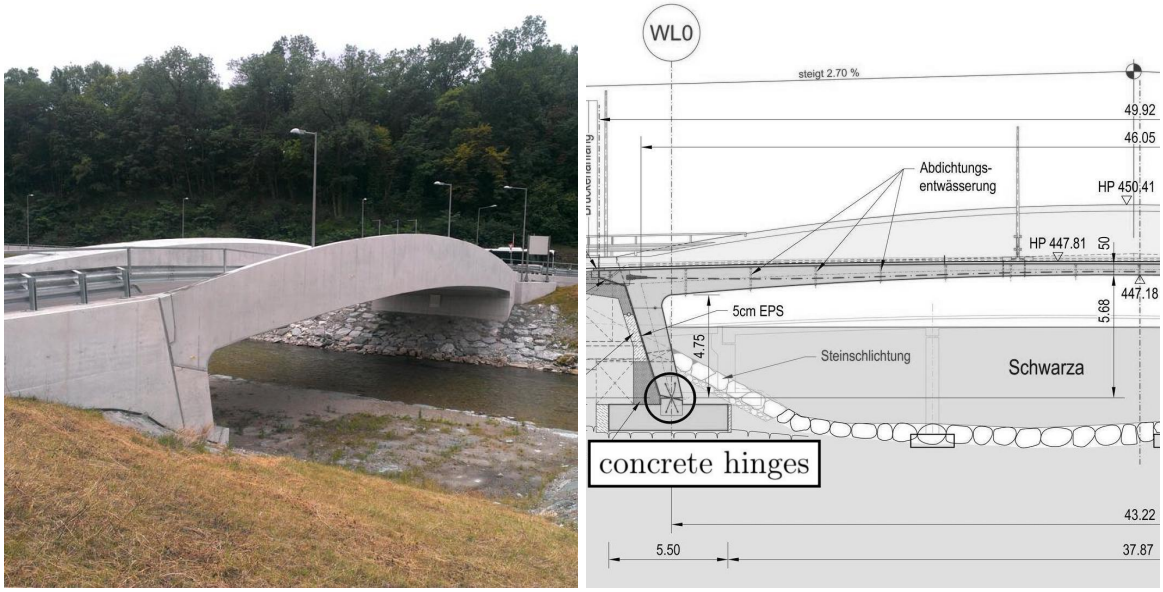

(a) (b)

Figure 16: (a) Photo of the Huyck-bridge, built in 2013/14, in Gloggnitz, Austria [41], and (b) one half of the longitudinal section, taken from [39], showing the positions of the reinforced concrete hinges

Table 4: Material properties of the concrete and the steel rebars and geometric dimensions of the two types of concrete hinges of the Huyck-bridge [40]

strength class for concrete: C30	$\|f_{ck}\|$	30 MPa
	E_{cm}	33 GPa
strength class for steel: B550	f_{yk}	550 MPa
	E_{sm}	200 GPa
geometric dimensions:	$a_1 = a_2$	150 mm
	b_1	2250 mm
	b_2	2650 mm
	c_1	3100 mm
	c_2	5275 mm
	$d_1 = d_2$	1000 mm
cross-sectional area of the reinforcement:	A_{s1}	12667 mm^2
	A_{s2}	16286 mm^2
reinforcement ratio:	ρ_1	3.75%
	ρ_2	4.10%
ratio of triaxial-to-uniaxial compressive strength:	F_1	2.03
	F_2	2.44

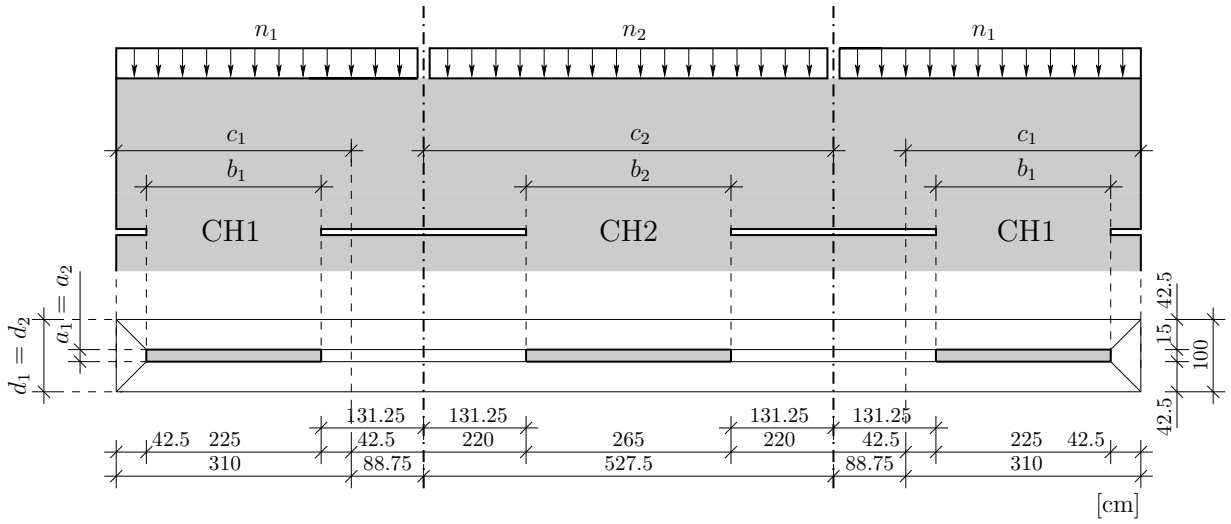

(a)

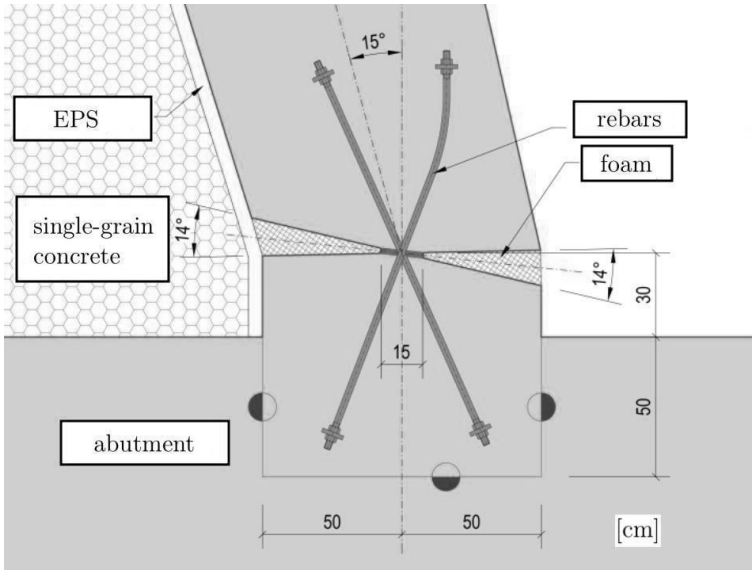

(b)

Figure 17: (a) Cross-sections through the necks of three neighboring concrete hinges, and (b) vertical section through one of the concrete hinges, showing the reinforcement crossing the neck [40]

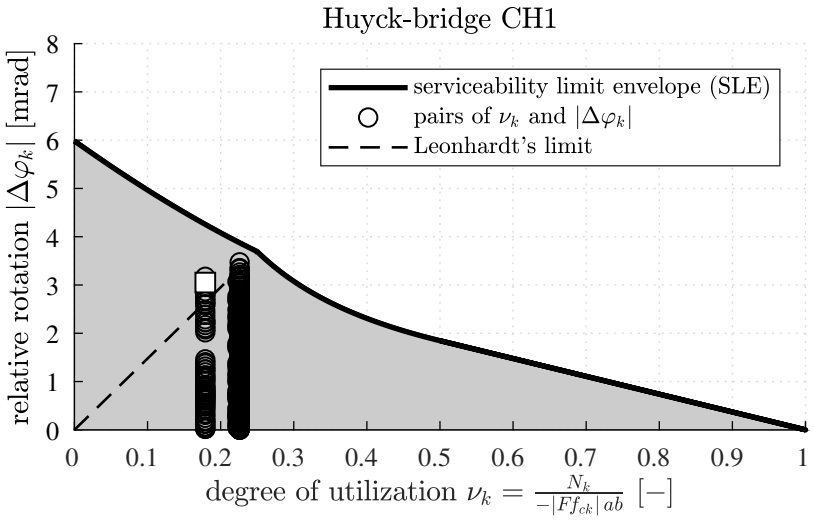

(a)

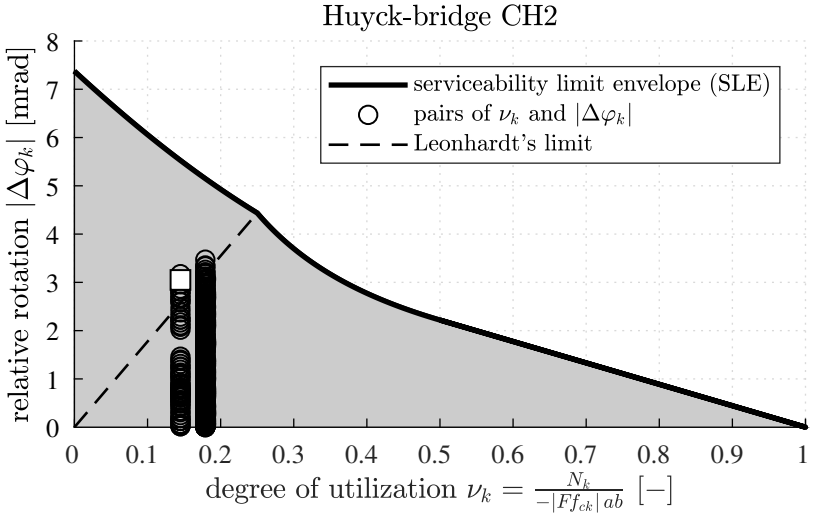

(b)

Figure 18: Dimensionless design diagram used for verification of serviceability limit states of the reinforced concrete hinges of the Huyck-bridge: relative rotations as a function of the degree of utilization of the normal force: concrete hinge (a) of type CH1 and (b) of type CH2; the squares highlight the combination of load cases (1) dead load, (2) prestress, (3) lateral soil pressure, (4) creep and shrinkage of concrete, (5) soil settlement of type B, and (10) temperature change of type B, see Table 5

Table 5: Normal forces and relative rotations of the reinforced concrete hinges of the Huyck-bridge, taken from [39, 40]

Load case	Load type	Notation	CH1 N [kN]	CH2 N [kN]	$\Delta\varphi$ [mrad]
1	permanent (G)	dead load	-3672	-4224	-3.36
2	permanent (P)	prestress	≈ 0	≈ 0	$+2.98$
3	permanent (G)	lateral soil pressure	≈ 0	≈ 0	$+0.12$
4	permanent (G)	creep/shrinkage	≈ 0	≈ 0	-1.16
5A	permanent (G)	soil settlement A	≈ 0	≈ 0	$+0.12$
5B	permanent (G)	soil settlement B	≈ 0	≈ 0	-0.60
6A	variable (Q)	traffic: load model 1 [36] A	-978	-999	-0.16
6B	variable (Q)	traffic: load model 1 [36] B	-978	-999	$+0.35$
7A	variable (Q)	traffic: load model 1 [36] horizontal A	≈ 0	≈ 0	$+0.14$
7B	variable (Q)	traffic: load model 1 [36] horizontal B	≈ 0	≈ 0	-0.14
8A	variable (Q)	lateral soil pressure resulting from traffic A	≈ 0	≈ 0	$+0.09$
8B	variable (Q)	lateral soil pressure resulting from traffic B	≈ 0	≈ 0	-0.12
9A	variable (Q)	traffic: load model 3 [36] A	-906	-852	$+0.38$
9B	variable (Q)	traffic: load model 3 [36] B	-906	-852	-0.02
10A	variable (Q)	temperature A	≈ 0	≈ 0	$+1.44$
10B	variable (Q)	temperature B	≈ 0	≈ 0	-2.04

the underlying mechanical model.

Finally, the maximum values of the bending moments that can be activated at the reinforced concrete hinges of the Huyck-bridge are obtained from Eq. (55). As for CH1 and CH2, they are given as

$$M_{k1,max} = 504\,\mathrm{kNm}\,, \tag{56}$$

and

$$M_{k2,max} = 627\,\mathrm{kNm}\,, \tag{57}$$

respectively. Although these values seem to be large from the viewpoint of the cross-sectional area of the concrete hinges, they are actually rather small in comparison to the maximum values of the bending moments of the frame bridge.

5. Discussion

Reinforced concrete hinges which are serviceable shall not run into a long-term durability problem. This provides the motivation for the following discussion, referring to nonlinear creep of concrete, fluctuations regarding temperature and relative humidity, and to the risk of corrosion of the steel rebars.

Subjected to compression, concrete creeps *linearly* provided the compressive stresses are smaller than or equal to 45% of the short-term compressive strength [17]. Subjected to larger load levels, the creep activity of concrete increases superlinearly with the degree of utilization, see [42] for uniaxial compression and [43] for triaxial compression. This is referred to as *nonlinear* creep. Acoustic emission measurements have clarified that it is related to microcracking [44], resulting in damage of the material [45]. Thus, nonlinear creep under permanent loading shall be avoided.

The permanent normal forces transmitted across concrete hinges of integral bridges result primarily from dead load of the structure. Constant normal forces lead to *creep* of concrete. In order to avoid nonlinear creep, the value of the permanent normal force, N_G, shall fulfill the condition

$$\sum_j \frac{N_{G,j}}{-|F f_{ck}|\,ab} \leq 0.45\,, \tag{58}$$

where the summation refers to all possible combinations of load cases, analogous to Eq. (51). The steel rebars are not considered in Eq. (58). They represent

a hidden reserve.

Fluctuating environmental factors such as the temperature and relative humidity represent a serious threat for the durability of reinforced concrete hinges. Proton nuclear magnetic resonance tests have shown that nanoscopic Calcium Silicate Hydrates release water upon heating and take up water upon cooling [46], in a spontaneous and reversible fashion. These water uptake/release characteristics of the smallest building blocks of the cement paste result in changes of effective pore pressures, which explain the anomalous thermal expansion behavior of the cement paste [47]. In the practically relevant interval of relative humidities from 40% to 80%, the thermal expansion of the cement paste is significantly larger than that of frequently used aggregates [48]. Therefore, daily temperature changes result in significant microscopic thermal stresses of mature concrete [49], representing a considerable durability issue. The described issue is one out of many important structural challenges resulting from temperature changes, see, e.g. [50, 51, 52, 53].

Short-term bending moments of concrete hinges, resulting from variable loads, may result in crack opening displacements which allow for transport of corrosion-inducing media to the central reinforcement. Therefore, it is recommended to use stainless steel for the rebars crossing the neck of the concrete hinge, in order to ensure their long-term durability. Such a type of steel is not standardly used in practice. It is more expensive than regular steel. Thus, it is recommended to check the availability and the price of stainless steel rebars already during the stage of preliminary design.

Finally, the limitations of the presented developments are discussed: The *linear* distribution of compressive normal stresses, resulting from the combination of the Bernoulli-Euler hypothesis with Hooke's law, underestimates stress peaks of an actually *nonlinear* stress distribution, see [3, 12, 14, 29]. Thus, inelastic material behavior must be expected in a small region of the neck, where triaxial compressive stress states prevail. Because ductile and hardening-type material behavior of concrete is to be expected, these inelastic effects are acceptable. In this context, it is worth mentioning that it was the assumption of a *linear* stress distribution, which rendered derivation of *analytical* formulae possible. The latter allow practitioners to produce dimensionless design diagrams which account, in a customized fashion, for specific geometric and material properties of reinforced concrete hinges.

6. Conclusions

The derived analytical formulae and the corresponding dimensionless design diagrams, expressing maximum tolerable relative rotations as a function of the normal force transmitted across reinforced concrete hinges, are useful estimates of serviceability limit states.[2] This was shown based on relationships between the normal force, the bending moment, and the relative rotation, obtained from structural testing of reinforced concrete hinges. These tests were carried out in four different laboratories. The uniaxial compressive strength of the used concretes ranged from 45 to 107 MPa. The experiments were carried out according to two different protocols:

- Eccentric compression tests: Minor nonlinearities were found up to the serviceability limits of relative rotations, and significant nonlinearities above them.
- Cyclic bending at a constant normal force: Minor residual relative rotations were found after test cycles that did not reach the maximum tolerable relative rotations, but significant residual deformations occurred after test cycles exceeding the serviceability limits.

Because the reinforcement was explicitly accounted for, the serviceability limits of relative rotations are *larger* than those according to the guidelines of Leonhardt and Reimann [6]. The proposed mechanical model allows for bending-induced tensile macrocracking *beyond* one half of the smallest cross-section of the neck, because tensile forces are activated in the rebars, which ensures the required position stability

[2] A parametric study is presented in the supplementary data file.

of the hinge. This has turned out to be beneficial to re-analysis of serviceability limit states of the Huyck-bridge.

The developed design recommendations agree with the following basic principles concerning verification of serviceability limit states according to the *fib* Model Code 2010 [37] and the Eurocode [17, 34, 35, 36]:

- *Linear-elastic* stress-strain relationships are used for concrete subjected to compression and steel subjected to tension.
- Accepting tensile macrocracking of concrete, the compressive stresses of concrete and the tensile stresses of steel must stay below the corresponding elastic limits.
- The triaxial compressive strength of concrete is estimated based on regulations of Eurocode 2 regarding partially loaded areas.
- Unfavorable choices are made when it comes to quantification of characteristic strength values. The latter are set equal to the expected strength plus or minus 8 MPa, depending on whether a larger or a smaller quantile of the strength leads to a more conservative design.
- Characteristic load combinations are estimated based on the regulations of the Eurocode.

These conclusions provide the motivation to use the proposed mechanical model also for drawing up recommendations for verification of ultimate limits. This is the topic of the companion paper [31].

Acknowledgments

Financial support of the experiments by the Austrian Ministry for Transport, Innovation and Technology (BMVIT), the Austrian Research Promotion Agency (FFG), ÖBB-Infrastruktur AG, and ASFINAG Bau Management GmbH, provided within VIF-project 845681 "Optimierte Bemessungsregeln für dauerhafte bewehrte Betongelenke", is acknowledged. The writers appreciate discussions with Alfred Hüngsberg, Andreas Schön, and Hannes Kari (ÖBB-Infrastruktur AG), Erwin Pilch and Michael Kleiser (ASFINAG Bau Management GmbH), as well as the communication of the technical report [40] by Oliver Einhäuser and Alfred Mayerhofer (PCD ZT-GmbH). Help of the laboratory staff, both at Vienna University of Technology (TU Wien) and Smart Minerals GmbH, by Wolfgang Dörner, Herbert Pardatscher, and Rudolf Dechet is particularly acknowledged.

Financial support by the Austrian Science Fund (FWF), provided within project P 281 31-N32 "Bridging the Gap by Means of Multiscale Structural Analysis", is also gratefully acknowledged.

Conflict of interest

The authors declare that they have no conflict of interest.

List of symbols

A	cross-sectional area of the neck
A_s	cross-sectional area of rebars crossing the neck
a	width of the neck, measured in the z-direction
a_c	compressed ligament of the neck
b	depth of the neck, measured in the y-direction
b_R	depth of the front-side notches, measured in the y-direction
c	depth of the adjacent reinforced concrete part, measured in the y-direction
d	width of the adjacent reinforced concrete part, measured in the z-direction
$\mathrm{d}A$	differential of A
$\mathrm{d}z$	differential of z
e	eccentricity of the normal force
E_c	Young's modulus of concrete
E_{cm}	mean value of E_c
E_s	Young's modulus of steel
E_{sm}	mean value of E_s
F	triaxial-to-uniaxial compressive strength ratio
F_a	factor accounting for lateral contraction of the neck
F_b	factor accounting for thickness contraction of the neck
f_c	uniaxial compressive strength of concrete

f_{ck} characteristic value of f_c
f_y yield stress of steel
f_{yk} characteristic value of f_y
M bending moment
M_k characteristic value of M
N normal force
N_k characteristic value of N
N_G contribution to N_k resulting from permanent loads
N_P contribution to N_k resulting from prestressing
N_Q contribution to N_k resulting from variable loads
t height of the throat of the neck, measured in the x-direction
u displacement component in the x-direction
x Cartesian coordinate
y Cartesian coordinate
z Cartesian coordinate
β opening angle of the throat of the neck
$\Delta\ell$ change of length of the neck
$\Delta\ell_\ell$ tolerable value of $\Delta\ell$
$\Delta\varphi$ relative rotation across the neck
$\Delta\varphi_\ell$ tolerable value of $\Delta\varphi$
$\Delta\varphi_{\ell k}$ characteristic value of $\Delta\varphi_\ell$
$\Delta\varphi_k$ characteristic value of $\Delta\varphi$
$\Delta\varphi_G$ contribution to $\Delta\varphi_k$ resulting from permanent loads
$\Delta\varphi_P$ contribution to $\Delta\varphi_k$ resulting from prestressing
$\Delta\varphi_Q$ contribution to $\Delta\varphi_k$ resulting from variable loads
ε axial normal strain component in the x-direction
ε_c ε of concrete
ε_s ε of steel
ν degree of utilization of N
ν_k characteristic value of ν
ρ reinforcement ratio
σ axial normal stress component in the x-direction
σ_c σ of concrete
σ_s σ of steel
χ flag, indicating whether steel is subjected to tension or compression
ψ_0 parameter, accounting for the probability that unfavorable non-permanent actions occur simultaneously

References

[1] E. Freyssinet, Le pont de Candelier [The bridge of Candelier], Annales des Ponts et Chaussées 1 (1923) 165f, (in French).

[2] E. Freyssinet, Naissance du béton précontraint et vues d'avenir [Birth of prestressed concrete and future outlook], Travaux (1954) 463–474, (in French).

[3] W. Kaufmann, T. Markić, M. Bimschas, Betongelenke - Stand der Technik und Entwicklungspotential [Concrete hinges - state of the art and potential for development], Verband der Schweizerischen Cementindustrie (cemsuisse) (2017) 1–19, (in German).

[4] J.-L. Zhang, T. Schlappal, Y. Yuan, H. Mang, B. Pichler, The influence of interfacial joints on the structural behavior of segmental tunnel rings subjected to ground pressure, Tunneling and Underground Space Technology 84 (2019) 538–556.

[5] J. Dix, Betongelenke unter oftmals wiederholter Druck- und Biegebeanspruchung [Concrete hinges subjected to frequently repeated axial compression and bending], Deutscher Ausschuß für Stahlbeton 150 (1962) 1–41, (in German).

[6] F. Leonhardt, H. Reimann, Betongelenke: Versuchsbericht, Vorschläge zur Bemessung und konstruktiven Ausbildung [Concrete hinges: experiments, design, and execution], Deutscher Ausschuß für Stahlbeton 175 (1965) 1–34, (in German).

[7] G. Franz, H.-D. Fein, Betongelenke unter wiederholten Gelenkverdrehungen [Concrete hinges under repeated hinge rotation], Deutscher Ausschuß für Stahlbeton 200 (1968) 56–91, (in German).

[8] M. Tourasse, Essais sur articulation Freyssinet [Experiments on Freyssinet hinges], Annales de l'Institute Technique du Bâtiment et des Travaux Publics 40 (57) (1961) 62–87, (in French).

[9] G.D. Base, Tests on a reinforced concrete hinge with a large design rotation, Cement and Concrete Association, 1962.

[10] E.O. Fessler, Die EMPA-Versuche an armierten Betongelenken für den Hardturm-Viadukt [EMPA-Experiments on reinforced concrete hinges for the Hardturm-Viadukt], Schweizer Bauzeitung 85 (1967) 623–630, (in German).

[11] D.A. Hordijk, F.B.J. Gijsbers, Projectbureau Boortunnels, Laboratoriumproeven tunnelsegmenten [Laboratory testing of tunnel segments], Reporte Interno K100-W-026 (1996), TNO-Bouw, Delft, (in Dutch).

[12] T. Schlappal, M. Schweigler, S. Gmainer, M. Peyerl, B. Pichler, Creep and cracking of concrete hinges – insight from centric and eccentric compression experiments, Materials and Structures 50 (6) (2017) 244.

[13] P. Janßen, Tragverhalten von Tunnelausbauten mit Gelenkstübbings [Structural behavior of segmented tunnel linings], Ph.D. thesis, Technical University of Braunschweig (1983), (in German).

[14] G.M.L. Gladwell, Contact problems in the classical theory of elasticity, Springer Science & Business Media, 1980.

[15] A. Caratelli, A. Meda, Z. Rinaldi, S. Giuliani-Leonardi, F. Renault, On the behavior of radial joints in segmental tunnel linings, Tunnelling and Underground Space Technology 71 (2018) 180–192.

[16] C.B.M. Blom, Design philosophy of concrete linings for tunnels in soft soils, Ph.D. thesis, Delft University of Technology (2002).

[17] British Standards Institution, CEN European Committee for Standardization, EN 1992-1-1:2015-07-31 Eurocode 2: design of concrete structures - part 1-1: general rules and rules for buildings (2015).

[18] B. Tvede-Jensen, M. Faurschou, T. Kasper, A modelling approach for joint rotations of segmental concrete tunnel linings, Tunnelling and Underground Space Technology 67 (2017) 61–67.

[19] X. Liu, Z. Dong, W. Song, Y. Bai, Investigation of the structural effect induced by stagger joints in segmental tunnel linings: Direct insight from mechanical behaviors of longitudinal and circumferential joints, Tunnelling and Underground Space Technology 71 (2018) 271–291.

[20] X. Li, Z. Yan, Z. Wang, H. Zhu, Experimental and analytical study on longitudinal joint opening of concrete segmental lining, Tunnelling and Underground Space Technology 46 (2015) 52–63.

[21] X. Li, Z. Yan, Z. Wang, H. Zhu, A progressive model to simulate the full mechanical behavior of concrete segmental lining longitudinal joints, Engineering Structures 93 (2015) 97–113.

[22] E. Mönnig, D. Netzel, Zur Bemessung von Betongelenken [Design of concrete hinges], Der Bauingenieur 44 (1969) 433–439, (in German).

[23] BE 5/75, Technical Memorandum (Bridges) Rules for the Design and Use of Freyssinet Concrete Hinges in Highway Structures, Design Manual for Roads and Bridges (1975).

[24] S. Marx, G. Schacht, Berechnungsmodelle für Betongelenke [Design models for concrete hinges], Prüfingenieur 36 (2010) 15–26, (in German).

[25] S. Marx, G. Schacht, Betongelenke im Brückenbau [Concrete hinges in bridge construction], Berlin Deutscher Beton- und Bautechnik Verein 18 (2010), (in German).

[26] ÖBV-Guideline, Guideline-Concrete Segmental Lining Systems, Austrian Society for Concrete and Construction Technology (2011).

[27] DAUB-Guideline, Recommendations for the design, production and installation of segmental rings, German Tunneling Committee (ITA-AITES) (2013).

[28] BAEL, Règles techniques de conception et de calcul des ouvrages et constructions en béton armé suivant la méthode des états limites [Technical rules for the design and calculation of reinforced concrete structures according to limit states], CSTB (2000), (in French).

[29] J. Kalliauer, T. Schlappal, M. Vill, H. Mang, B. Pichler, Bearing capacity of concrete hinges subjected to eccentric compression: multiscale structural analysis of experiments, Acta Mechanica 229 (2) (2018) 849–866.

[30] ÖBV-communication, Bautechnik 2016 [Structural engineering 2016], Austrian Society for Construction Technology (2016), (in German).

[31] T. Schlappal, J. Kalliauer, M. Vill, H. Mang, J. Eberhardsteiner, B. Pichler, Ultimate limits of reinforced concrete hinges, Submission intended to Engineering Structures.

[32] S. Gmainer, M. Vill, B. Pichler, T. Schlappal, J. Kalliauer, Optimierte Bemessungsregeln für dauerhafte bewehrte Betongelenke ["Optimized design rules for durable reinforced concrete hinges"], Final project report, FFG, Austrian Research Funding Agency, Vienna, Austria, (in German) (2016).

[33] G. Schacht, N. Hoffmann, S. Marx, Federgelenke: Anwendung im Hoch-und Brückenbau [Use of semi-articulations in structural and bridge engineering], Stahlbau 82 (12) (2013) 903–910, (in German).

[34] British Standards Institution, CEN European Committee for Standardization, EN 1990:2013-03-15 Eurocode - Basis of structural design (2013).

[35] British Standards Institution, CEN European Committee for Standardization, EN 1990/A1:2013-03-15 Eurocode - Basis of structural design - Amendment 1: Application for bridges (2013).

[36] British Standards Institution, CEN European Committee for Standardization, EN 1991-2:2012-03-01 Eurocode 1: Actions on structures - Part 2: Traffic loads on bridges (2012).

[37] Comité Européen du Béton, Fédération Internationale de la Précontrainte (CEB-FIP), *fib* Model Code for Concrete Structures 2010, Ernst & Sohn, Wiley, 2013.

[38] H. Müller, I. Anders, R. Breiner, M. Vogel, Concrete: treatment of types and properties in fib Model Code 2010, Structural concrete 14 (4) (2013) 320–334.

[39] PCD ZT-GmbH, Huyckbrücke [Huyck-bridge], Accessed: 2018-11-08, (in German).
URL `https://www.pcd-zt.at/projekte/br%C3%BCcken/huyckbr%C3%BCcke/`

[40] PCD ZT-GmbH: Einhäuser, O, Semmering Basistunnel, Baulos PGG1-Vorhaben Gloggnitz; Straßenbrücke Huyckstraße über die Schwarza; 2010-024, Unpublished technical report (2013), (in German).

[41] Revotec ZT-GmbH, Referenzen [References], Accessed: 2018-12-11, (in German).
URL `https://www.revotec.at/de/referenzen`

[42] M. Ruiz, A. Muttoni, P. Gambarova, Relationship between nonlinear creep and cracking of concrete under uniaxial compression, Journal of Advanced Concrete Technology 5 (2007) 383–393.

[43] S. Ullah, B. Pichler, S. Scheiner, C. Hellmich, Shell-specific interpolation of measured 3D displacements, for micromechanics-based rapid safety assessment of shotcrete tunnels, Computer Modeling in Engineering and Sciences (CMES) 57 (3) (2010) 279.

[44] P. Rossi, J.-L. Tailhan, F. Le Maou, L. Gaillet, E. Martin, Basic creep behavior of concretes investigation of the physical mechanisms by using acoustic emission, Cement and Concrete Research 42 (1) (2012) 61–73.

[45] I. Fischer, B. Pichler, E. Lach, C. Terner, E. Barraud, F. Britz, Compressive strength of cement paste as a function of loading rate: Experiments and engineering mechanics analysis, Cement and Concrete Research 58 (2014) 186–200.

[46] M. Wyrzykowski, P. J. McDonald, K. L. Scrivener, P. Lura, Water redistribution within the microstructure of cementitious materials due to temperature changes studied with ^{1}H NMR, The Journal of Physical Chemistry C 121 (50) (2017) 27950–27962.

[47] H. Wang, C. Hellmich, Y. Yuan, H. Mang, B. Pichler, May reversible water uptake/release by hydrates explain the thermal expansion of cement paste?—Arguments from an inverse multiscale analysis, Cement and Concrete Research 113 (2018) 13–26.

[48] J. H. Emanuel, J. Hulsey, Prediction of the thermal coefficient of expansion of concrete, Journal of the American Concrete Institute 74 (4) (1977) 149–155.

[49] H. Wang, H. Mang, Y. Yuan, B. L. Pichler, Multiscale thermoelastic analysis of the thermal expansion coefficient and of microscopic thermal stresses of mature concrete, Materials 12 (17) (2019) 2689.

[50] T. Yi, H. Li, M. Gu, Full-scale measurements of dynamic response of suspension bridge subjected to environmental loads using GPS technology, Science China Technological Sciences 53 (2) (2010) 469–479.

[51] D.-H. Yang, T.-H. Yi, H.-N. Li, Y.-F. Zhang, Correlation-based estimation method for cable-stayed bridge girder deflection variability under thermal action, Journal of Performance of Constructed Facilities 32 (5) (2018) 04018070.

[52] D.-H. Yang, T.-H. Yi, H.-N. Li, Coupled fatigue-corrosion failure analysis and performance assessment of RC bridge deck slabs, Journal of Bridge Engineering 22 (10) (2017) 04017077.

[53] H.-B. Huang, T.-H. Yi, H.-N. Li, H. Liu, New representative temperature for performance alarming of bridge expansion joints through temperature-displacement relationship, Journal of Bridge Engineering 23 (7) (2018) 04018043.